國立交通大學

顯示科技研究所

碩士論文

反射式顯示器之均勻前光照明系統設計與應用

Study of Front Illuminating Systems for Reflective Displays

研究生：莊浩彣

指導教授：田仲豪 副教授
黃乙白 助理教授

中華民國 九十八 年 六 月

反射式顯示器之均勻前光照明系統設計與應用

Study of Front Illuminating Systems for Reflective Displays

研 究 生：莊浩彣　　Student : Hao-Wen Chuang
指導教授：田仲豪　　Advisor : Chung-Hao Tien
黃乙白　　Yi-Pai Huang

國立交通大學
顯示科技研究所
碩士論文

A Thesis
Submitted to Display Institute
College of Electrical Engineering
National Chiao-Tung University
in Partial Fulfillment of the Requirements
for the Degree of
Master
in

Display Institute

June 2009

Hsinchu, Taiwan, Republic of China

中華民國 九十八 年 六 月

反射式顯示器之均勻前光照明系統設計與應用

碩士研究生：莊浩彣　　指導教授：田仲豪 副教授
黃乙白 助理教授

國立交通大學　　顯示科技研究所

摘　要

近年來隨著顯示技術的發展，膽固醇反射式液晶顯示器開始應用於大型電子看板。反射式顯示器不需要背光源，而是利用周圍的環境光源作為照明來源以顯示影像，因此反射式顯示器的影像品質與環境照明密切相關，在戶外陽光充足或明亮的環境下能擁有好的影像品質，但當使用於夜晚時或昏暗的室內環境下，由於不足的照明度而需要提供一前光照明給顯示看板。然而，常見的照明燈具例如MR lamp，自斜向的照射角度造成顯示器表面亮度不均勻，影響影像品質。

本論文研究提出一以均勻照明為目標的前光照明設計。此燈具設計使用CCFL 作為光源，利用自由型式的鏡面反射罩來分佈光線，均勻地照射在目標顯示器上。根據燈源與目標平面的距離，照射範圍，及燈源與目標平面之間的相對位置，以數值分析計算出所需的自由型式反射罩的形狀。模擬結果驗證所設計的照明系統明顯地改善照明均勻度，均勻度偏移量在 5%內。初步的燈具模型的製作方法與實驗結果，以及實際照射在膽固醇液晶顯示器上的效果，在論文中有詳細的討論與分析。

Study of Front Illuminating Systems for Reflective Displays

Master Student: Hao-Wen Chuang **Advisors: Dr. Chung-Hao Tien**
Dr. Yi-Pai Huang

Display Institute
National Chiao Tung University

Abstract

Recently, Cholesteric reflective LCDs have been applied to electronic billboards. Reflective LCDs, without the back-light source, utilize ambient light as the main source for illumination. The image qualities of electronic billboards are ideal in well-lit locations or under diffuse sunlight. At night or in dim indoor environments, front lighting is necessary due to insufficient surrounding illumination. However, conventionally available Luminaires, such as MR lamps, generally illuminate the display with non-uniform brightness, resulting in poor image quality.

A front-lighting design for uniform illumination was proposed. The Luminaire applies a free-form mirror surface reflector to redistribute light from the CCFL source. The shape of the free-form reflector was numerically calculated according to the normal distance between the source and the target plane, the illuminated region, and the positions of the source and the target plane. Simulation results show that the proposed illuminating system improves illumination uniformity where uniformity deviation is within 5%. Fabrication and experimental results for a Luminaire prototype, and demonstration on a Cholesteric LCD, are discussed and analyzed.

誌　謝

首先感謝田仲豪老師與黃乙白老師在我碩班兩年中予我的指導與訓練，包括論文研究的邏輯思考與組織報告的能力，以及提供良好的研究環境與資源，讓我順利完成論文，獲益良多。

感謝洪健翔學長在研究上細心的指導與協助，在無數次的討論過程中給予我許多實用的建議。實作方面，感謝江松柏學長、學校機械工廠莊先生、光峰科技陳信安先生、金益世黃信道先生諸位的協力與幫忙。也感謝實驗室同學，靖堯、博文、積賢及鳳玲在實驗上的協助。

實驗室的生活多采多姿，留下許多難忘的回憶。感謝芳正學長、喬舜學長及均合學長的照顧，還有一群同甘共苦的同學們，宜如、宗緯、佑禎、拓江、宜伶、俊賢，以及致維、育誠等其他同學們在課業與生活上的切磋。研究上的辛苦與煩悶隨著歡笑聲而煙消雲散。

最後感謝我的父母親的支持與鼓勵，讓我無後顧之憂地完成學業。在此致上我最誠摯的感謝。

Table of Contents

Figure Captions

List of Tables

Chapter 1

Introduction and Objective

To begin with, the background for illumination systems and lighting Luminaires are briefly introduced. Then lighting considerations on reflective displays are discussed. Finally, the objective and organization of this thesis are stated.

1.1 Illumination system

Unlike imaging optics which pursues the qualities of forming an image, non-imaging optics is concerned with optimal transfer of light radiation from a source to a target. Non-imaging optics design is extensively applied to the field of solar energy concentration, backlights for liquid crystal displays, fiber optics illumination devices, and reflectors and lenses Luminaire. (Fig. 1-1)

Reflective illumination systems

In terms of reflective-type illumination systems, reflectors are the core components. Traditionally, common shapes of reflectors are conic surfaces which are specified by a conic constant k. The analytical equations for these conic surfaces are straightforward and few parameters are varied for certain optical performance. The illumination principles of parabolic, elliptical and spherical reflectors are illustrated in Fig. 1-2. These surfaces are easily manufactured and polished precisely.

Recently, thanks to progress in manufacturing technology, more free-form reflectors are used in illumination systems, especially in those with asymmetric light

distribution; for example, vehicle headlamp and sidewalk light. (Fig. 1-3) Free-form surface is defined as any non-rotationally symmetric surface or a symmetric surface which rotates about any axis that is not its symmetrical axis. Free-form surfaces offer more degrees of freedom for design and make the illumination system more compact than rotationally symmetric surfaces.

Headlamp

Solar concentrator

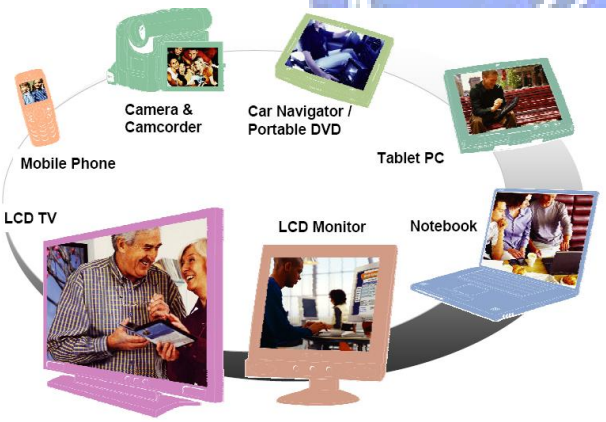

Backlight for LCD

Shadowless lamp for operating

Fig. 1-1 Non-imaging optics applications [1][2]

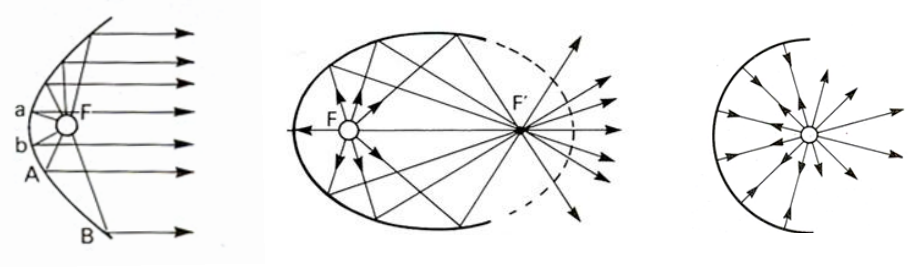

$k = -1$ $\quad -1 < k < 0$ $\quad k = 0$

Fig. 1-2 Conic surface reflectors

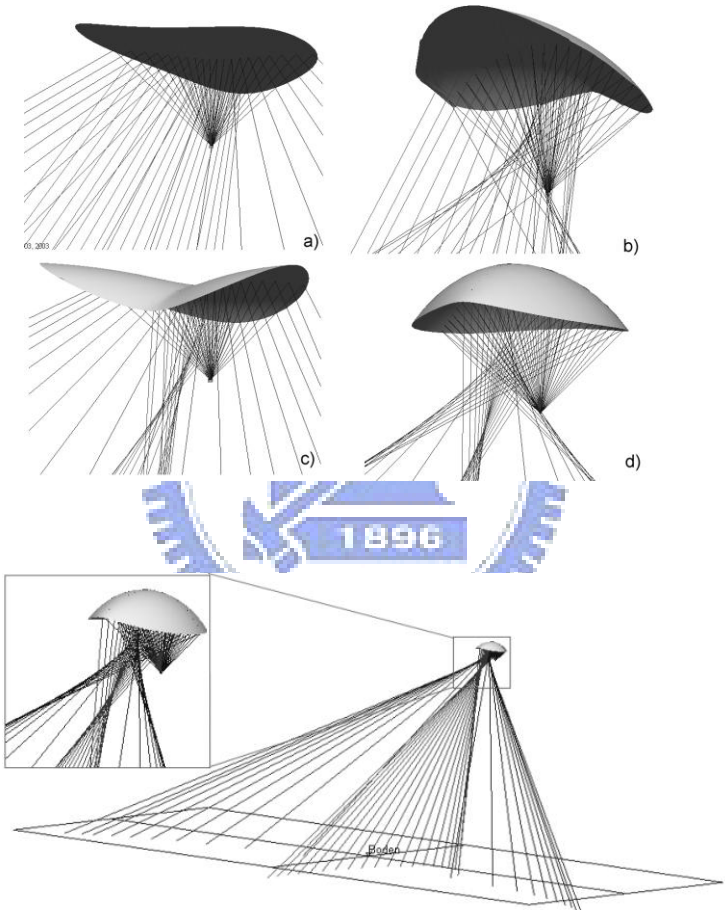

Fig. 1-3 Free-form mirror reflector for sidewalk light [3]

1.2 Lighting Luminaires

Lighting plays a crucial role in our daily life. Lighting provides human visual

needs as well as safety and security. In addition, lighting has strong social and emotional significance.

Since Thomas Edison invented the first commercially practical incandescent electric light bulb in 1879, the world has become brighter. A revolution in lighting occurred in 1938 when General Electric Corporation developed the fluorescent lamp which rendered more energy efficiency and longer lifetime than the incandescent lamp. With the development of lighting technology, fluorescent lamps have continually improved and are now widely applied to the general lighting equipment in commercial and institutional buildings. (Fig. 1-4)

Fig. 1-4 Light sources for general lighting [4]

Luminaire is an electrical device that creates artificial light or illumination on the target region. Effective lighting can distribute appropriate light on the required region and eliminate light where it's not needed. For various lighting purposes or in different locations, Luminaires utilize optical components to exhibit light distribution for specific applications. Electric Luminaires generally consist of the following parts: sources, ballasts, reflectors, shielding or diffusion components, and housings. The

reflectors redirect most of the light emitted from the lamp and produce a desired light distribution. The optical properties of reflector materials can be specular, spread, or diffuse as shown in Fig. 1-5. Specular materials permit precise redirection of light rays and sharp cutoffs, while painted reflectors produce diffuse, scattered, or widespread light distribution. The high-reflectance materials with about 98% reflectivity can enhance lighting efficiency.

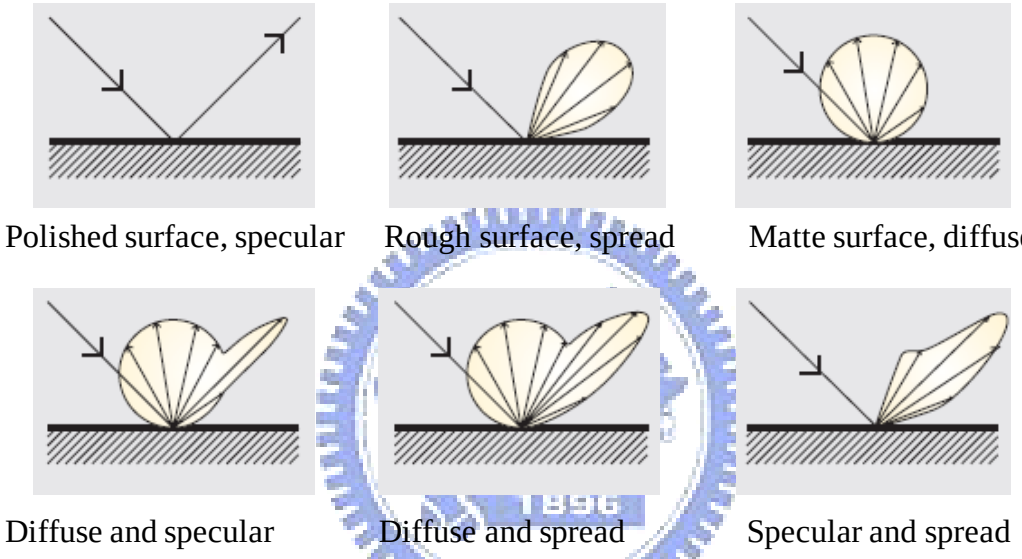

Fig. 1-5 Reflector materials and optical properties [4]

The scattered radiance distribution for an ideal diffuse surface is Lambertian. The distribution of scattered intensity is given by the following equation,

$$I(\theta) = I_0 \cdot \cos(\theta) \tag{1.1}$$

as illustrated in Fig. 1-6(a). The Gaussian distribution for a rough surface is shown in Fig. 1-6(b), and the distribution of scattered intensity varies according to the equation

$$I(\theta) = I_0 \cdot \exp[-\frac{1}{2}(\frac{\theta}{\sigma})^2], \tag{1.2}$$

where I_0 is the intensity in the specular direction, σ is the standard deviation of the Gaussian distribution.

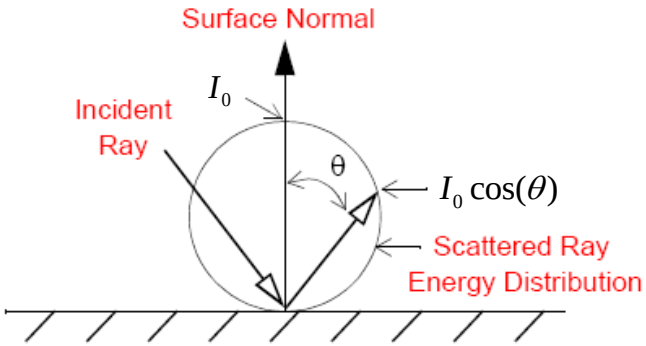

(a)

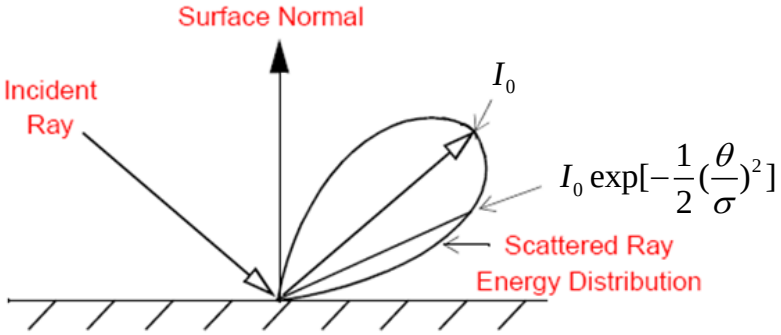

(b)

Fig. 1-6 (a) Lambertian distribution for a diffuse surface (b) Gaussian distribution for a rough surface

1.3 Lighting considerations on reflective displays

The reflective color Liquid Crystal Display (LCD) was proposed by T. Uchida in 1995. Reflective LCDs, without the back-light source, utilize ambient light as the main source for illumination. As shown in Fig. 1-7, the reflector which is formed on one of pair of substrates reflects ambient light to display images. Reflective LCDs have been widely used as mobile information display devices, such as mobile phones and personal digital assistants (PDAs).

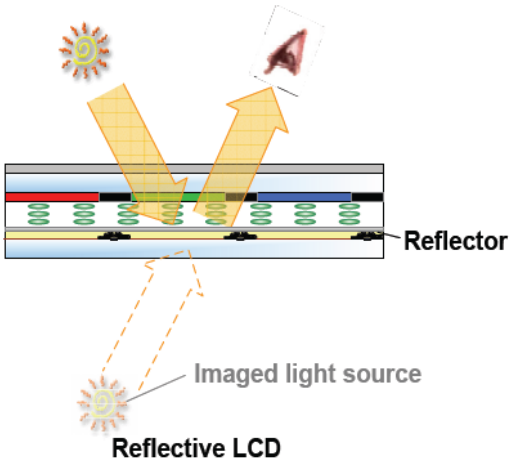

Fig. 1-7 Schematic illustration of a reflective type LCD [5]

One important reflective LCD technology is the Cholesteric LCD (Ch-LCD) for e-books. Recently, Ch-LCD has been applied to electronic billboards. The pictures shown in Fig. 1-8 are the full color reflective displays. They present the images under different illumination levels.

Fig. 1-8 Full color Cholesteric electronic billboards [6]

For electric billboards or electric poster applications, the lighting for reflective displays is critical. The image qualities of electronic billboards are ideal in well-lit

locations or under diffuse sunlight. At night, or in dim indoor environments, front lighting is necessary due to insufficient surrounding illumination. When applying front lighting to a reflective display, conventionally available Luminaires such as MR lamps (Fig. 1-9) generally lead to undesirable issues including non-uniform brightness and glare effect, which consequently hinders its use from high image and lighting quality.

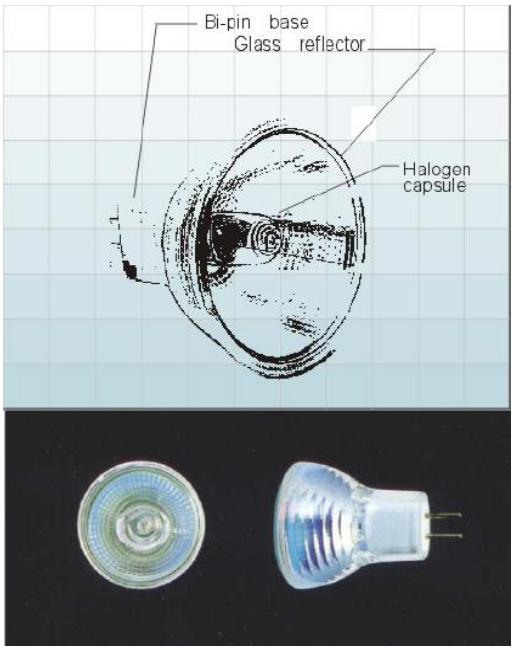

Fig. 1-9 MR16 and MR8 lamps [4] (MR stands for Multifaceted Reflector and the number is the diameter of cup in 1/8 inch)

1.4 Motivation and objective of this thesis

Due to the above lighting issues for reflective displays, in this thesis a front illuminating system for bright and uniform illumination was proposed. Different from MR lamp which utilizes tungsten-halogen incandescent light source, the proposed

Luminaire design uses CCFL (cold cathode fluorescent lamp) as the light source.

A free-form mirror surface reflector redistributes light from the source and then illuminates the target display uniformly. The shape of the free-form reflector is numerically calculated according to the determined normal distance between the source and the target plane, the illuminated region, and their relative positions. Optical performance including illuminance and illumination uniformity are evaluated using simulation tools.

1.5 Organization of this thesis

This thesis is organized as follows: The principles of illumination systems are presented in **Chapter 2**. In **Chapter 3**, the design concepts and mathematical model are described. Practical design case and simulation results are illustrated in **Chapter 4.** In **Chapter 5**, the fabrication methods and results of the prototype are shown, and experimental results are discussed. Finally, conclusions and recommendations for the future work are presented in **Chapter 6**.

Chapter 2

Principles of Illumination Systems

For the purpose of designing and analyzing illumination systems, several optical principles are described in this chapter. Rays emitted from light source pass through an optical system following the principles of geometrical optics. Ray-tracing results are mainly interpreted by Radiometry and Photometry quantities, and illumination uniformity on the target plane is defined to evaluate the performance of the illumination system.

2.1 Laws of refraction and reflection

Light is an electromagnetic wave phenomenon. As the wavelength of light is much smaller than surrounding objects it propagates through and around, the behavior of light can be approximated and described by ray optics (geometrical optics). In geometrical optics, light travels in the form of rays and obeys a set of geometrical rules including laws of refraction and reflection.

Law of refraction (Snell's law)

When a light ray is incident on a boundary surface of two media where the refractive indices of the two media are n_i and n_t, the ray is split into a reflected ray and a refracted (transmitted) ray as shown in Fig. 2-1. The incident ray, the normal direction of the surface, and the refracted ray all lie in the same plane called incident plane. The propagating direction of the refracted ray follows the relationship,

$$n_i \sin\theta_i = n_t \sin\theta_t, \tag{2.1}$$

where θ_i is the angle between the incident ray and the normal direction of the surface (the incidence angle) and θ_t is the angle between the refracted ray and the surface normal (the refraction angle). This relationship is called Snell's law and can be proved by Fermat's Principle. [7]

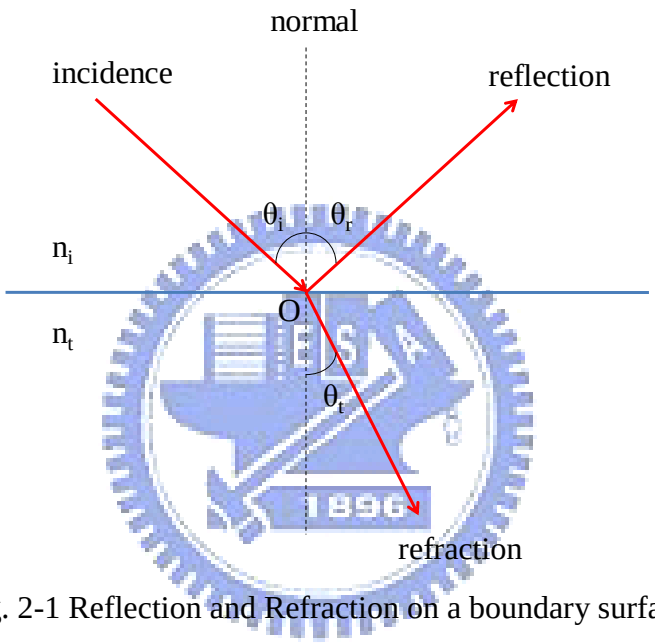

Fig. 2-1 Reflection and Refraction on a boundary surface

Law of reflection

The reflected light lies in the incident plane and possesses an angle θ_r with respect to the normal direction of the surface. The angle of reflection is equal to the angle of incidence,

$$\theta_i = \theta_r, \tag{2.2}$$

which is called the law of reflection.

Therefore, the propagating direction of a light ray in an optical system can be traced and calculated.

2.2 Radiometry and Photometry quantities

2.2.1 Radiometry

Radiometry is the science of measurement of electromagnetic radiation. Some fundamental quantities which characterize the energy content of radiation are summarized in Table 2-1. [8]

Table 2-1 Energy-based units

Quantity	Symbol	Definition	SI Units
Radiant energy	Q_e	--	Joule
Radiant flux	Φ_e	dQ_e/dt	Watt
Radiant exitance	M_e	$d\Phi_e/dA$	$Watt/m^2$
Irradiance	E_e	$d\Phi_e/dA$	$Watt/m^2$
Radiant intensity	I_e	$d\Phi_e/d\Omega$	Watt/sr
Radiance	L_e	dI_e/dA	$Watt/sr \cdot m^2$

From the above table, Q_e is the energy of a collection of photons while the energy of a single photon is hν. Radiant exitance M_e pertains to radiation leaving a surface; Irradiance E_e pertains to radiation incident on a surface. Radiant intensity I_e is the radiant flux Φ_e emitted per unit of solid angle Ω by a point source in a given direction. The Radiance L_e indicates the radiant intensity per unit of projected area perpendicular to the light of sight as shown in Fig. 2-2.

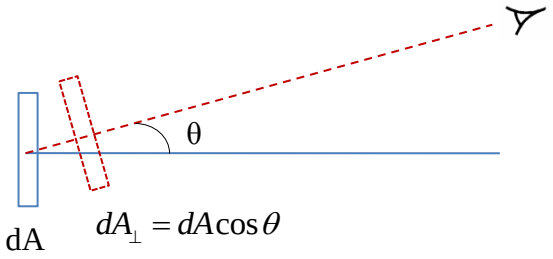

Fig. 2-2 Definition of projected area

2.2.2 Photometry

Compared to Radiometry that measures all radiant energy, Photometry applies only to the visible portion of the optical spectrum for the human eye. Since the human eye does not respond with equal sensitivity at all wavelengths of visible light, the radiant power at each wavelength is weighted by CIE luminous efficiency curve which models human brightness sensitivity. The standard model that represents response or sensation of brightness for the eye versus wavelength is reproduced in Fig. 2-3.

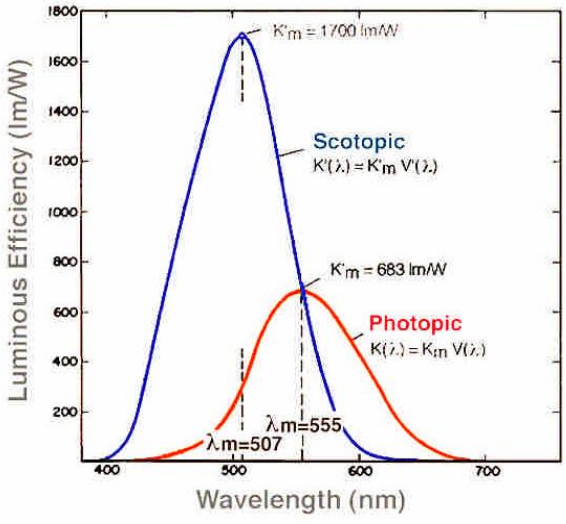

Fig. 2-3 Scotopic and Photopic spectral sensitivities

Photometric quantities are related to Radiometric quantities through the

luminous efficiency curve. One watt of radiant energy at the wavelength of maximum visual sensitivity (555 nm) is defined to be 683 lumens. Thus, the luminous flux emitted from a source with a radiant flux $\Phi_\lambda(\lambda)$ is given by

$$\Phi_v(\lambda) = 683 \text{ lm/w} \cdot \int V_\lambda(\lambda)\Phi_\lambda(\lambda)d\lambda \tag{2.3}$$

where $\int V_\lambda(\lambda)$ is the normalized Luminous efficiency depicted in Fig. 2-4. Some Photometric units parallel to stated Radiometric units are illustrated in Table 2-2.

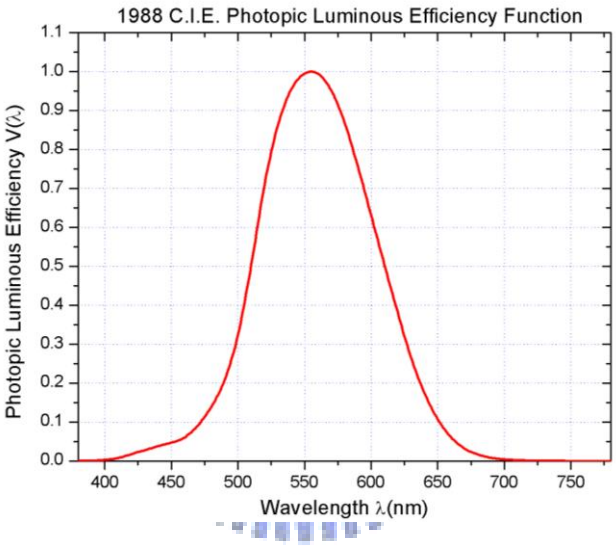

Fig. 2-4 1988 CIE Photopic Luminous Efficiency Function [9]

Table 2-2 Photon-based Units

Quantity	Symbol	Definition	SI Units
Luminous energy	Q_v	--	lumen • s
Luminous flux	Φ_v	dQ_v/dt	lumen (lm)
Luminous exitance	M_v	$d\Phi_v/dA$	lumen /m^2
Illuminance	E_v	$d\Phi_v/dA$	lumen /m^2 or lux
Luminous intensity	I_v	$d\Phi_v/d\Omega$	lumen /sr or candela
Luminance	L_v	$dI_v/dA_\perp$	lumen/sr • m^2 or nits

2.2.3 $\cos^3\theta$ Law

For example, assumed that there is a point source with luminous intensity Is illuminating on a screen, and z is the normal distance from the source to the screen shown in Fig. 2-5. Then the illuminance of the detected area dA_d on the screen is derived from

$$d\Phi_d = I_s \cdot d\Omega = I_s \cdot \frac{dA_d \cos\theta}{r^2}, \tag{2.4}$$

$$d\Phi_d = I_s \cdot \frac{dA_d \cos\theta}{(z/\cos\theta)^2}, \tag{2.5}$$

$$E_d = \frac{d\Phi_d}{dA_d} = \frac{I_s \cos^3\theta}{z^2}. \tag{2.6}$$

That is, the illuminance on the screen is proportional to $\cos^3\theta$ where $\cos\theta = \frac{z}{r}$. The relationship is called $\cos^3\theta$ Law.

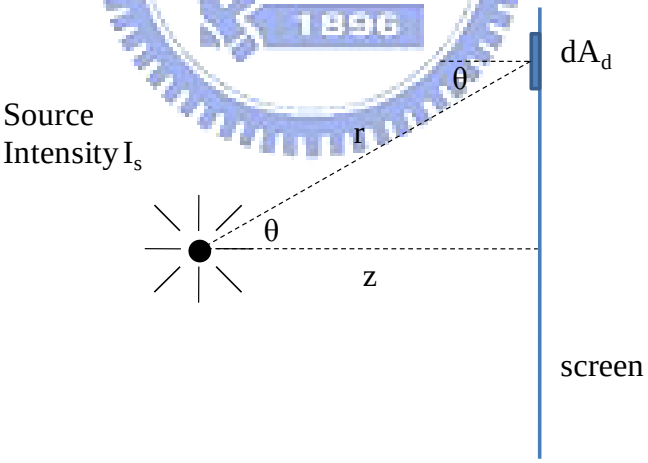

Fig. 2-5 $\cos^3\theta$ Law illustration

2.3 Etendue theorem

Etendue or étendue is an optical invariant of an optical system. It specifies geometric capability of an optical system that transmits radiation, or its optical throughput. In a perfect optical system without any losses from reflections, absorptions, or scattering, the etendue is a constant. The radiance of an optical system is equal to the derivative of the radiant flux with respect to the étendue.

Generalized Etendue theory which was developed by Welford (1974) is introduced in the following. [10] It is assumed that any ray is traced through an optical system as illustrated in Fig. 2-6. Any two points P and P' are located in the entry and exit spaces at Cartesian coordinates (x, y) and (x', y'), respectively. Eikonal V is defined as the optical path length from P to P' along the physically possible paths. V is multi-valued if there are more than one ray passing through P and P' and then V is a function of x, y, x', and y'. The direction cosines of the ray in the two spaces are described as (L, M, N) and (L', M', N').

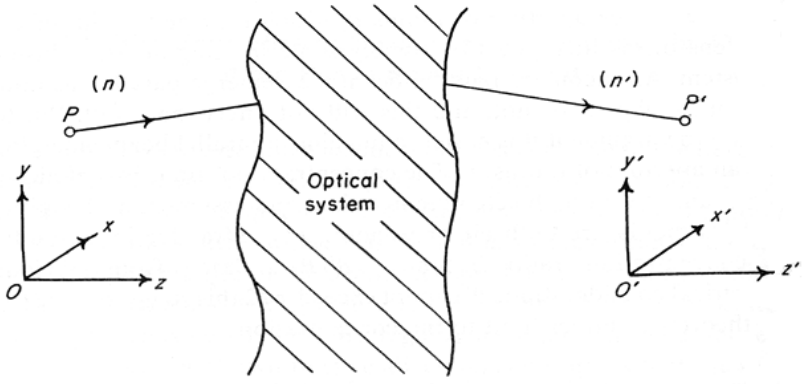

Fig. 2-6 Proof of Etendue theorem

According to the fundamental property of the eikonal, we have

$$\begin{aligned} &\partial V/\partial x = -nL,\ \ \partial V/\partial y = -nM, \\ &\partial V/\partial x' = -n'L',\ \ \partial V/\partial y' = -n'M', \end{aligned} \tag{2.7}$$

where n and n' are refractive indices of entry and exit spaces, respectively.

Extend to two-dimensional and differentiate Eq. (2.7) again, we obtain

$$\begin{aligned} dp &= -V_{xx}dx - V_{xy}dy - V_{xx'}dx' - V_{xy'}dy' \\ dq &= -V_{yx}dx - V_{yy}dy - V_{yx'}dx' - V_{yy'}dy' \\ dp' &= -V_{x'x}dx + V_{x'y}dy + V_{x'x'}dx' + V_{x'y'}dy' \\ dq' &= -V_{y'x}dx + V_{y'y}dy + V_{y'x'}dx' + V_{y'y'}dy' \end{aligned} \tag{2.8}$$

where

$$p = n \cdot L,\ q = n \cdot M. \tag{2.9}$$

After a sequence of mathematical manipulation, these terms can be put into a matrix form,

$$\begin{pmatrix} V_{xx'} & V_{xy'} & 0 & 0 \\ V_{yx'} & V_{yy'} & 0 & 0 \\ V_{x'x'} & V_{x'y'} & -1 & 0 \\ V_{y'x'} & V_{y'y'} & 0 & -1 \end{pmatrix} \begin{pmatrix} dx' \\ dy' \\ dp' \\ dq' \end{pmatrix} = \begin{pmatrix} -V_{xx} & -V_{xy} & -1 & 0 \\ -V_{yx} & -V_{yy} & 0 & -1 \\ -V_{x'x} & -V_{x'y} & 0 & 0 \\ -V_{y'x} & V_{y'y} & 0 & 0 \end{pmatrix} \begin{pmatrix} dx \\ dy \\ dp \\ dq \end{pmatrix}. \tag{2.10}$$

Eq. (2.10) can be denoted as matrices A, B and the column vectors M,

$$BM' = AM. \tag{2.11}$$

Multiplying through by the inverse of B,

$$M' = B^{-1}AM. \tag{2.12}$$

Then Eq. (2.12) can be expanded and rewritten as Eq. (2.13) with three similar equations,

$$dx' = \frac{\partial x'}{\partial x}dx + \frac{\partial x'}{\partial y}dy + \frac{\partial x'}{\partial p}dp + \frac{\partial x'}{\partial q}dq. \tag{2.13}$$

Since Eq. (2.13) is the determinant of the matrix $B^{-1}A$ as well as the Jacobian,

$$\det(B^{-1}A) = \frac{\partial(x', y', p', q')}{\partial(x, y, p, q)} \tag{2.14}$$

which transforms the differential four-volume $dxdydpdq$. Thus,

$$dx'dy'dp'dq' = \frac{\partial(x', y', p', q')}{\partial(x, y, p, q)} dxdydpdq = dxdydpdq \tag{2.15}$$

because of the unity value of the Jacobian.

Therefore, the optical invariant of any system is proved,

$$n'^2 dx'dy'dL'dM' = n^2 dxdydLdM. \tag{2.16}$$

The invariant in Eq. (2.16) shall be interpreted in another way. (x, y, p, q) is treated as coordinates in a four-dimensional space and U is any enclosed volume in the space. Then U is given by

$$\int dU = \int\int\int\int dxdydpdq, \tag{2.17}$$

which indicates the invariant property.

2.4 Illumination uniformity evaluation index

The illumination uniformity can be evaluated by means of two methods. The first method is familiar to the evaluation rule for LCD backlight systems.[11] As shown in Fig. 2-7, thirteen positions on the target plane are chosen as measuring points to calculate the uniformity where

$$\text{Uniformity} = \frac{\text{minimum Illuminance (1~13)}}{\text{average Illuminance (1~9)}} \times 100\%. \tag{2.18}$$

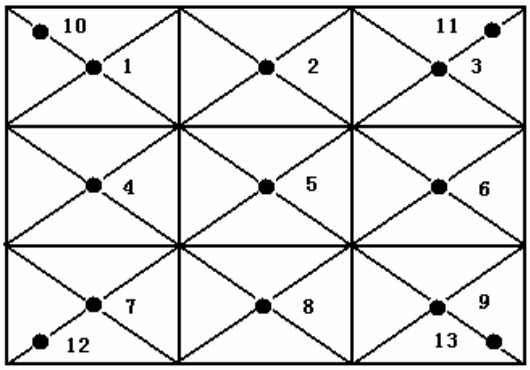

Fig. 2-7 Positions of measuring points

The other evaluation method characterizes illumination uniformity by calculating the uniformity deviation δ. [12]

$$\delta = \frac{\frac{1}{n}\cdot\sum_{i=1}^{n}\left|E_i - \overline{E}\right|}{\overline{E}} \tag{2.19}$$

where $\overline{E}$ is the average illuminance of number n samplings on the target plane. The illumination uniformity is superior when the uniformity deviation δ is smaller.

The first evaluation method is applicable on the basis of that there are no apparent dark or bright regions on the target plane, so the uniformity evaluated from these chosen measuring points are meaningful. In this research, the second method is preferable since more measuring points can ensure the uniformity evaluation to be more accurate.

Chapter 3

Front Lighting Modeling

The Luminaire is put in front and above the target display to provide downward illumination. (Fig. 3-1) Vertical light distribution on the target plane is not uniform with the upper plane receiving more light. To simplify optical analysis and reflector design, a two-dimensional analysis is investigated in the following.

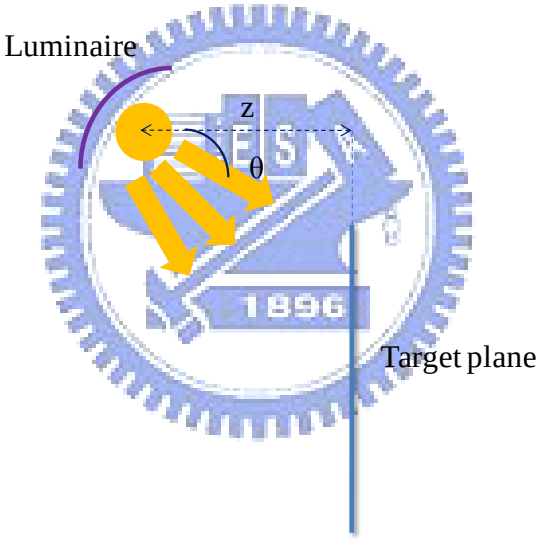

Fig. 3-1 Sketch of Luminaire and illuminated target plane

3.1 Design model in terms of Etendue

Modeling of front light reflector with a free-form curvature for uniform illumination is described. The luminous flux from the light source is adjusted by variable curvatures of the reflector curve and then the flux is redistributed as an

expected light distribution on the target plane.

3.1.1 Target light intensity distribution

Referred to $\cos^3\theta$ Law illustrated in section 2.2.3, the illuminance on the target plane is a function of the angle θ,

$$E_d = I_s \cdot \frac{\cos^3\theta}{z^2}, \tag{3.1}$$

which is not uniform.

If the illuminance on the target plane is defined to be a constant E_0 everywhere, that is, uniform illumination, then the luminous intensity distribution is derived as a function of the inverse of the cosine θ cube, where

$$I_s(\theta) = \frac{E_0 \cdot z^2}{\cos^3\theta}. \tag{3.2}$$

3.1.2 Concept

Geometric configurations of the light source and the reflector shape are illustrated in Fig. 3-2. It is assumed that the linear light source is placed at the origin and perpendicular to the drawing plane. Light rays emit uniformly from the source and then reflect on the surface of the reflector.

The radiuses of curvature for different points on the reflector curve are not the same, resulting in variant ray diverging control. Luminous flux (ΔΦ) which is contained in an angle dθ falls onto the reflector curve, then it reflects and projects on the target plane with a diverging angle dθ'. Using Etendue concept, because of flux conservation, luminance is inversely proportional to the projected area and diverging angle. Thus, the luminance can be adjusted by the diverging angle corresponding to the arbitrary curvature of the reflector.

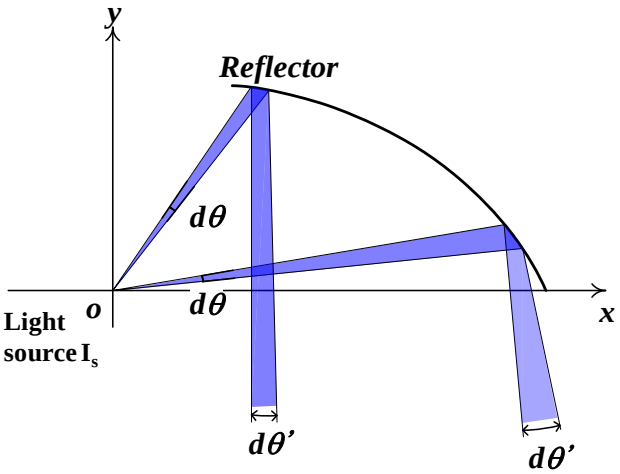

Fig. 3-2 Geometric configurations of the light source and the reflector with free-form curvature

The original luminous flux from the source is a conservation of the flux after being reflected from the reflector curve, so

$$\Phi = \int I_s \cdot d\theta = \int I' \cdot d\theta', \tag{3.3}$$

where I' is the target light intensity distribution derived from Eq. (3.2). I' was approximated as emitting from a point source.

3.2 Linear model

Compared to the Etendue model, the linear model is easier for calculation but is subjected to some conditions. The light source is assumed to emit equal light intensity in all directions. An example of that is the CCFL (cold cathode fluorescent lamp), which can be regarded as a point source for two-dimensional analysis.

Geometric configurations of the light source and the shape of the reflector are illustrated in Fig. 3-3. The linear light source is placed at point S (0,-d) and

perpendicular to the drawing plane. Light rays emit uniformly from the linear source and then reflect from the surface of the reflector. The incident ray angle θ is defined beginning on the y-axis. The illuminated target region Q is put at distance L from the origin.

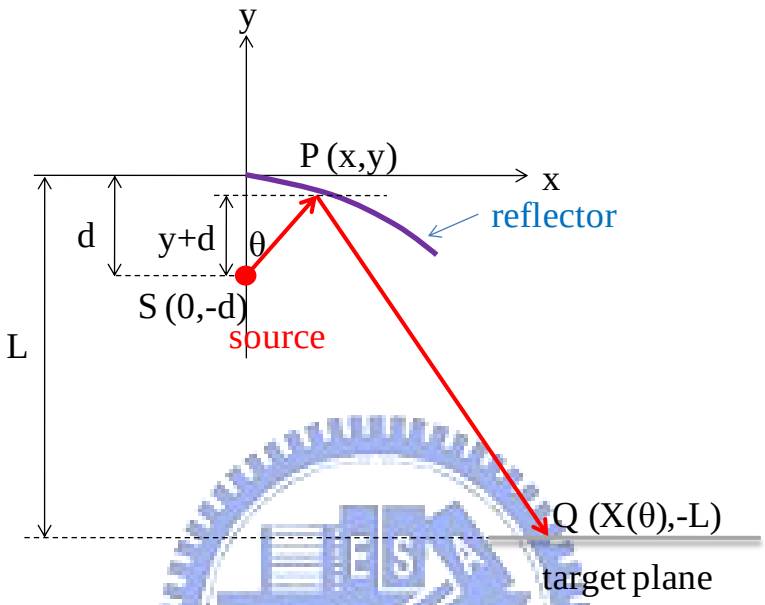

Fig. 3-3 Geometric analysis for linear design model

Using vector form and the assumed point-source for the two-dimensional analysis, incident and reflected ray vectors can be described as $\overrightarrow{SP} = (x, y+d)$ and $\overrightarrow{PQ} = (X(\theta)-x, -L-y)$, respectively. The tangent vector at a moving point P on the reflector curve can be derived from

$$\vec{T} = \frac{\overrightarrow{SP}}{\left|\overrightarrow{SP}\right|} + \frac{\overrightarrow{PQ}}{\left|\overrightarrow{PQ}\right|}, \tag{3.4}$$

so the differential equation for the reflector curve is written as

$$y' = \frac{\vec{T}\cdot\hat{y}}{\vec{T}\cdot\hat{x}} = \frac{\dfrac{y+d}{\sqrt{x^2+(y+d)^2}} + \dfrac{-L-y}{\sqrt{(X(\theta)-x)^2+(L+y)^2}}}{\dfrac{x}{\sqrt{x^2+(y+d)^2}} + \dfrac{X(\theta)-x}{\sqrt{(X(\theta)-x)^2+(L+y)^2}}}. \tag{3.5}$$

After substitution and simplification, Eq. (3.5) yields

$$\frac{dy}{d\theta} = \frac{y+d}{1-\tan\theta \cdot \frac{dy}{dx}} \cdot \frac{1}{\cos^2\theta} \cdot \frac{dy}{dx} \tag{3.6}$$

where

$$\frac{dy}{dx} = \frac{\cos\theta \cdot \sqrt{[X(\theta)-(y+d)\cdot\tan\theta]^2+(y+L)^2} - (y+L)}{\sin\theta \cdot \sqrt{[X(\theta)-(y+d)\cdot\tan\theta]^2+(y+L)^2} + [X(\theta)-(y+d)\cdot\tan\theta]} \tag{3.7}$$

For uniform illumination on the target region, $X(\theta)$ is linear to θ, that is,

$$X(\theta) = c\cdot\theta + X_0 \tag{3.8}$$

where c is a constant and $X(0) = X_0$.

As long as initial conditions, d, L, and the uniformly illuminated region Q is determined, the resulting reflector curve can be numerically calculated by the Runge-Kutta Method, which is a numerical analysis and will be introduced in the next section.

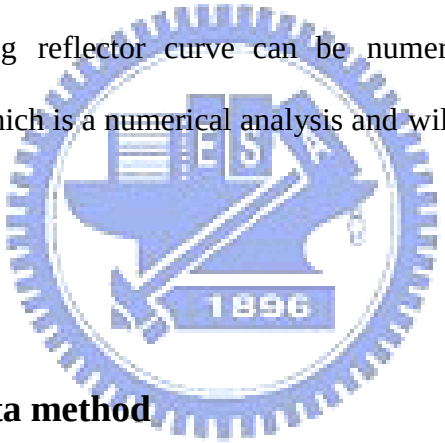

3.3 The Runge-Kutta method

The common fourth-order Runge–Kutta method [13][14] is a family of implicit and explicit iterative methods for approximation of solutions for ordinary differential equations.

The initial value problem is specified as

$$y' = f(\theta, y),\ y(\theta_0) = y_0. \tag{3.9}$$

Then the fourth-order Runge–Kutta method for this problem is given by the following equations

$$\begin{aligned} y_{n+1} &= y_n + \frac{h}{6}(K_1 + 2K_2 + 2K_3 + K_4) \\ \theta_{n+1} &= \theta_n + h \end{aligned} \tag{3.10}$$

where

$$
\begin{aligned}
K_1 &= f(\theta_n, y_n) \\
K_2 &= f(\theta_n + \frac{h}{2}, y_n + \frac{h}{2} K_1) \\
K_3 &= f(\theta_n + \frac{h}{2}, y_n + \frac{h}{2} K_2) \\
K_4 &= f(\theta_n + h, y_n + hK_3).
\end{aligned}
\tag{3.11}
$$

The next value y_{n+1} is determined by the present value y_n, plus the product of the size of interval h and an estimated slope. It is noted that above method is often referred to as "RK4". It is a fourth-order method, meaning that the error per step is on the order of h^5, while the total accumulated error has order h^4.

Chapter 4

Practical Design Case

Based on the mathematical model explained in section 3.2, the shape of the reflector could be derived using determined conditions. First, the flow chart for design is illustrated. Then selection of parameters and solutions for a free-form reflector curve for the illuminating target is presented. Simulation results together with discussions are shown as follows.

4.1 Flowchart

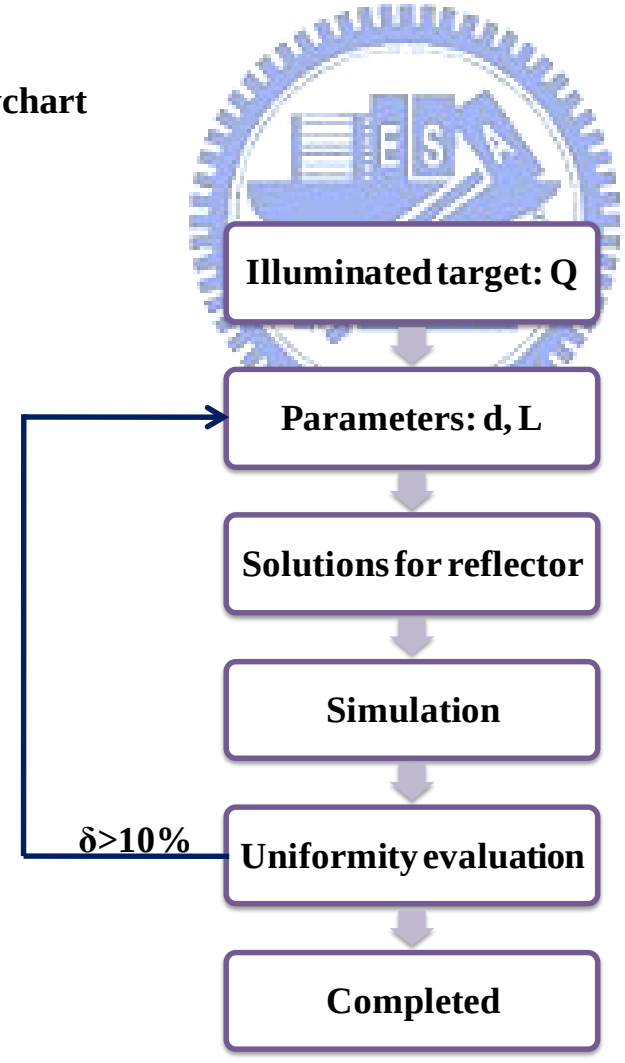

4.2 Illuminating target

A practical design case which is aimed at the uniform illumination region whose area is 50 cm x 40 cm^2 is shown in Fig. 4-1.

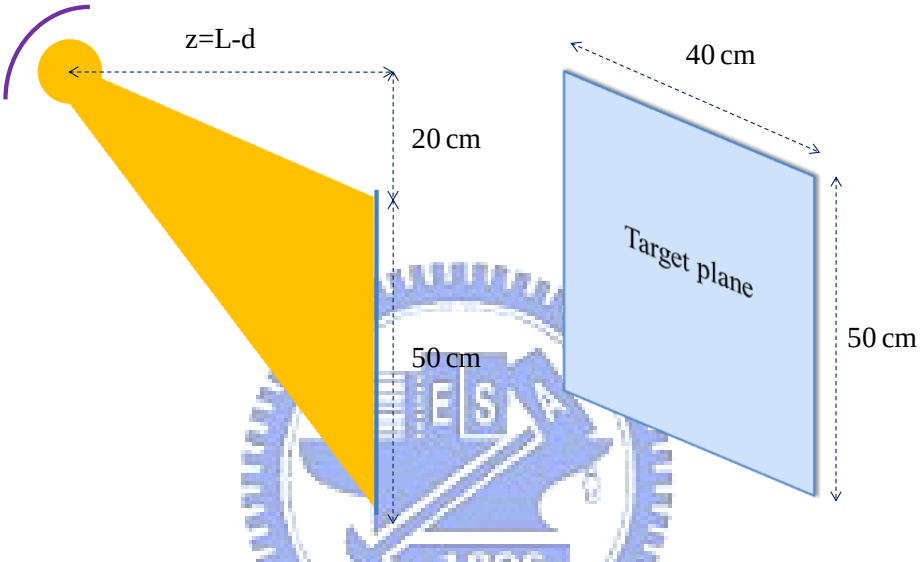

Fig. 4-1 Sketch of the practical design case

4.3 Selection of parameters

As shown in Fig. 4-2, according to the linear model described in section 3.2, the shape of the reflector can be derived from the following three initial conditions. d is the distance between the source and the origin. L is the distance between the target plane and the origin. Q is the illuminated region.

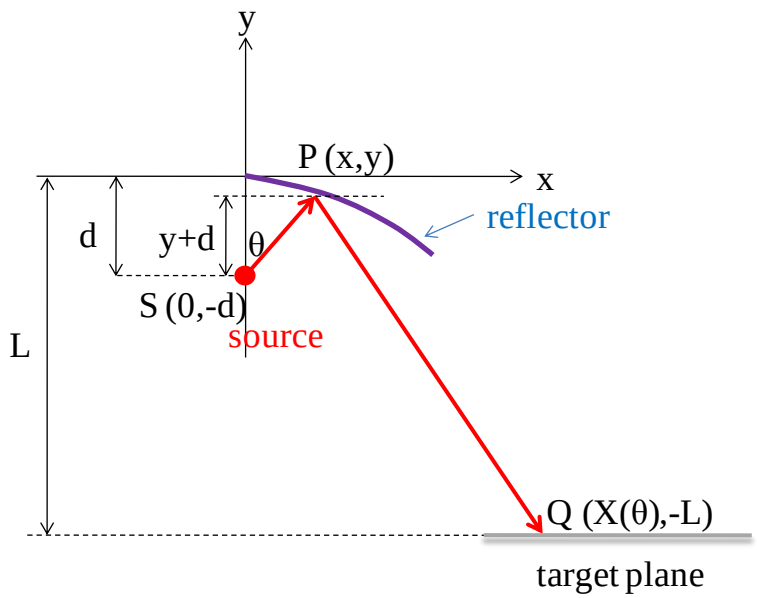

Fig. 4-2 Geometric analysis for linear design model

d is the distance between the source and the starting point (or the origin) of the reflector, designated as 5 cm. For the practical case, the illuminated region Q is 50 cm. L is the distance from the origin to the target plane and can be determined by the following. According to numerical analysis for solving the reflector curve, the relationship between distance L and the width of the reflector (or extension of the reflector in the positive x direction) is depicted in Fig. 4-3. Since the illuminated region is 50 cm (in the positive x direction), the reflector width at distance L=55 cm is considered to be the preferable choice for appropriate reflector width.

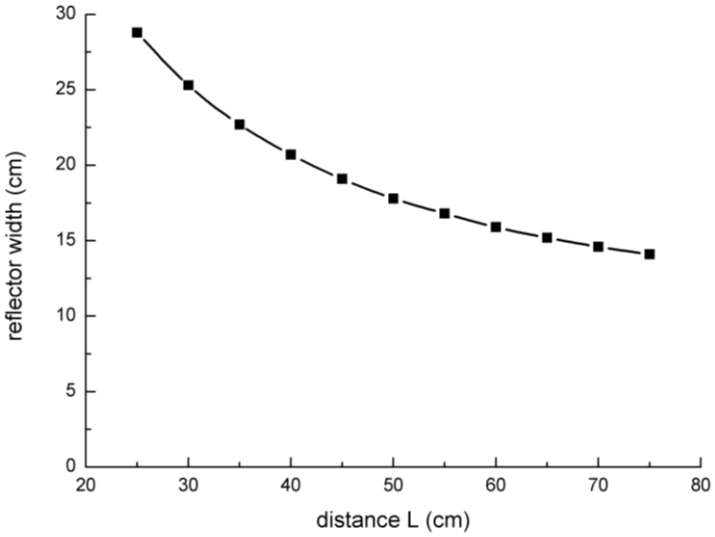

Fig. 4-3 Reflector widths at different distances L

4.4 Numerical solutions for a free-form reflector

When L=55 cm and d=5 cm, the free-form reflector curve could be solved by using numerical analysis, the Runge–Kutta method, which was introduced in section 3.3. The numerical solutions for Eq. (3.6), Eq. (3.7), and Eq. (3.8) were fitted through spline interpolation. Thus, the curve shown in Fig. 4-4 is the result of the free-form reflector shape, where the source is located at point S (0,-5).

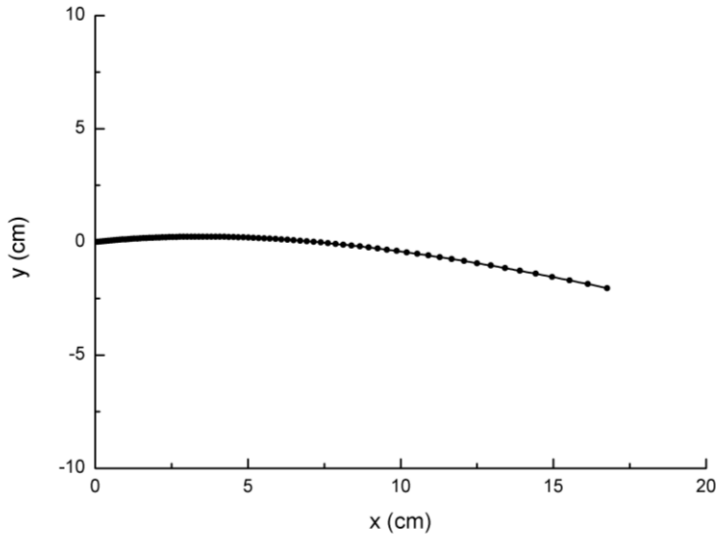

Fig. 4-4 Solutions for the free-form reflector shape

4.5 Simulation results and analysis

Optical simulation software LightTools® [15] was used to verify the mathematical model and evaluate optical performance of illumination systems. Cold Cathode Fluorescent Lamp (CCFL) was applied in the illumination system. With the assumption of the two-dimensional design and analysis model explained in section 3.2, light emitted from the smaller diameter (2 mm) of the CCFL tube was regarded as a point source relative to the reflector and the target plane. CCFL and the free-form mirror surface reflector were constructed by LightTools. Based on Monte Carlo ray tracing, reflected light was detected by the receiver on the target plane, and illuminance was calculated. Configurations of the CCFL source (located at the origin) and the free-form reflector as well as ray-tracing results are shown in Fig. 4-5.

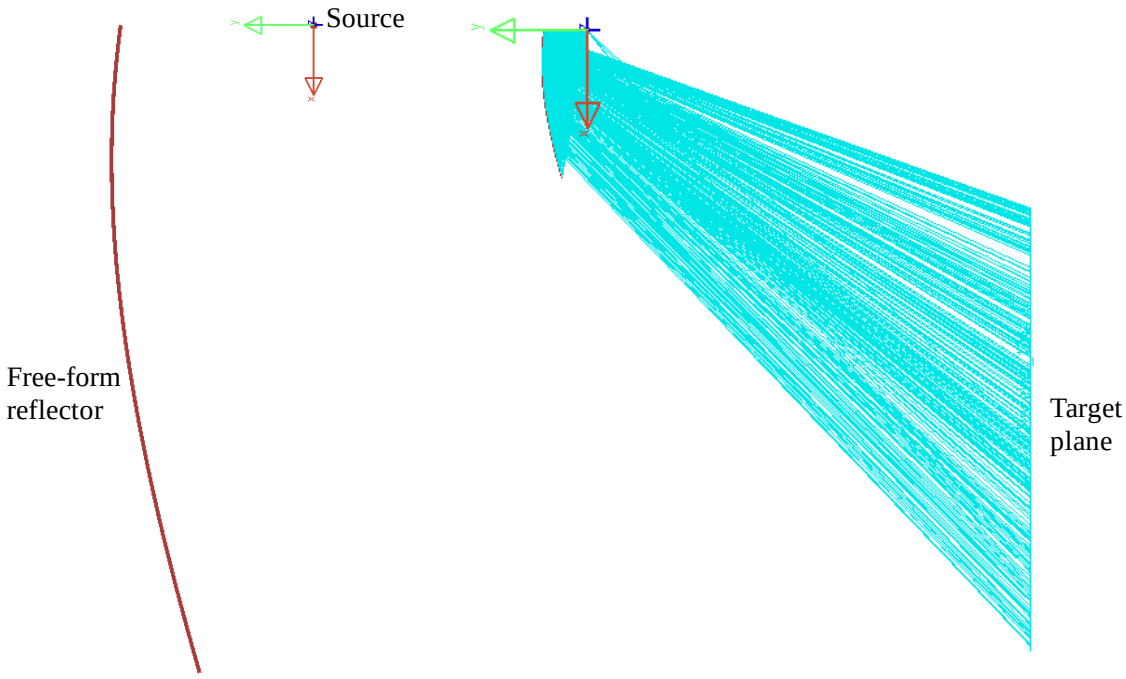

Fig. 4-5 (a) Configurations of the CCFL source (located at the origin) and the free-form reflector (b) ray-tracing results

The illuminance distribution chart of the free-form reflector illumination system is shown in Fig. 4-6. Compared to the illuminance distribution chart in Fig. 4-7, where CCFL was directly illuminating the plane, illumination uniformity was improved by the free-form reflector redistributing light from the CCFL source. The uniformity deviation was 8 %, where the uniformity deviation was defined in section 2.4. In addition, the average illuminance $\overline{E}$ of the free-form illumination system was enhanced to 111 Lux while the average illuminance of CCFL directly illuminating case was 63 Lux. Thus, the mathematical model was verified.

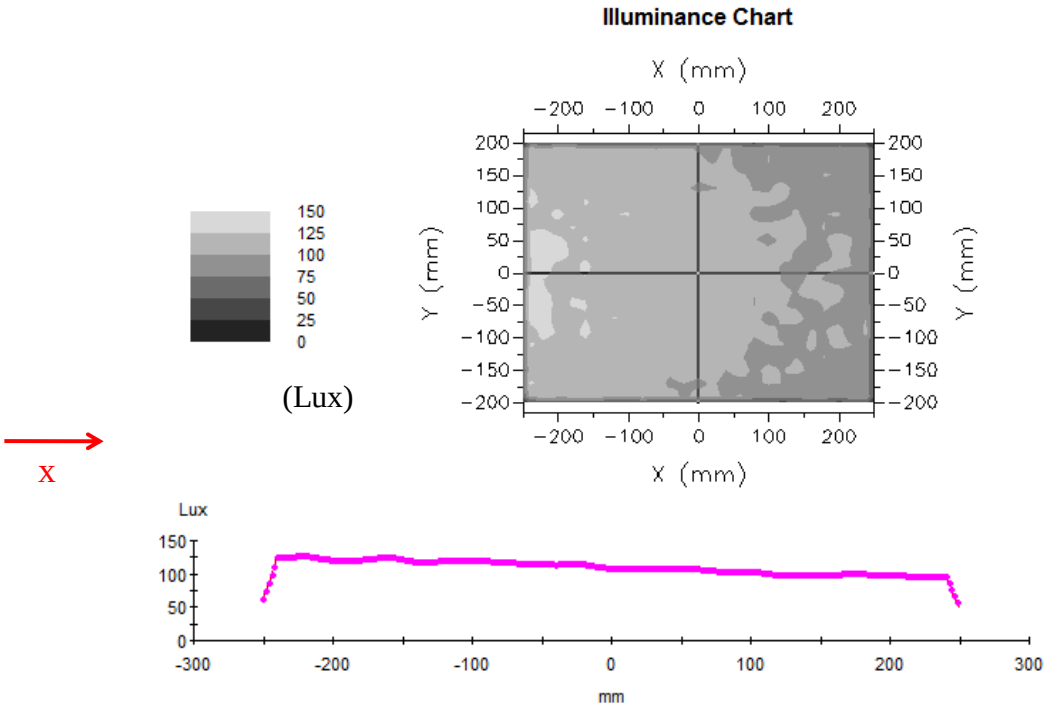

Fig. 4-6 Illuminance chart of the illumination system composed of the CCFL and the free-form reflector

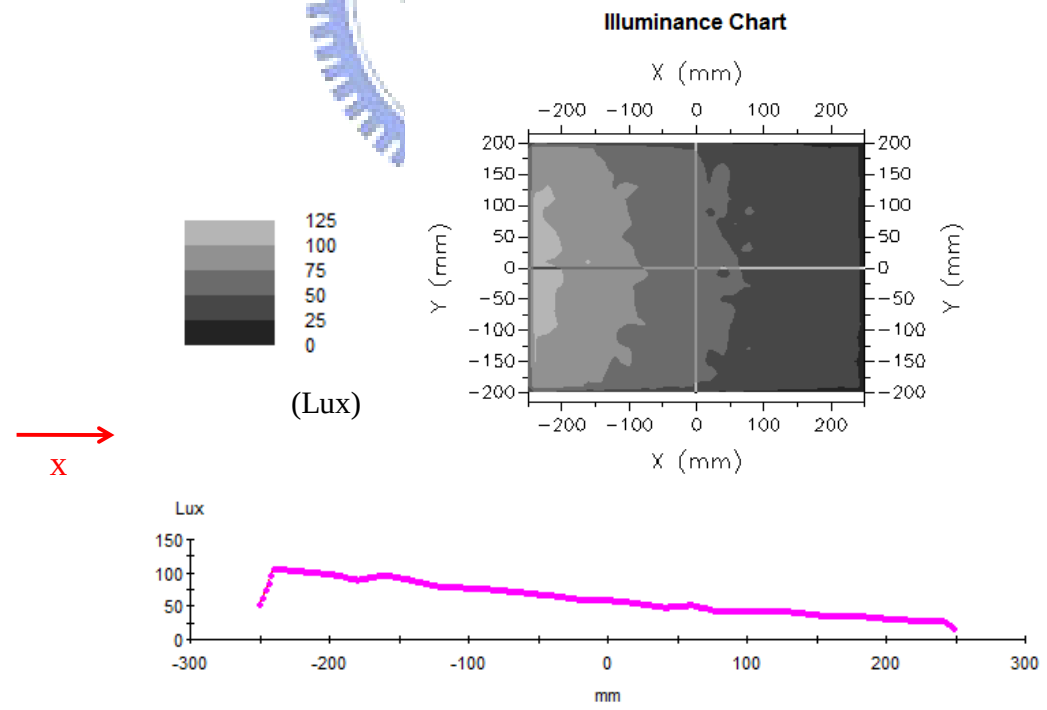

Fig. 4-7 Illuminance chart of the case where CCFL is directly illuminating

Moreover, the illuminance on the target plane was improved through increasing the use of light emitted from the source. A half circular lamp reflector shown in Fig. 4-8 (a) was included to reflect and reuse the light, and the circular reflector did not affect the output light distribution from the source. Configurations of the lamp refletor and the free-form reflector are shown in Fig. 4-8 (b).

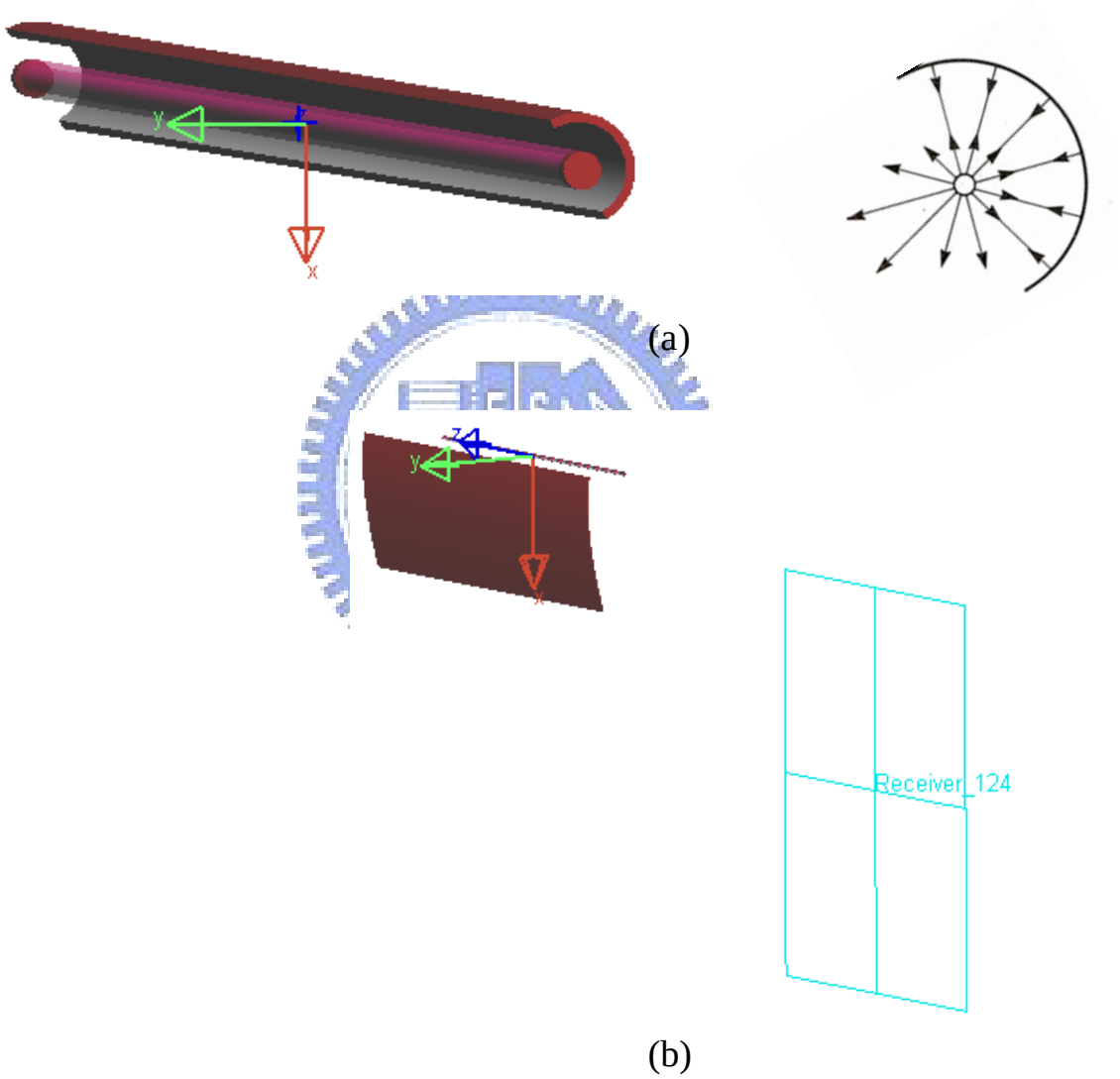

Fig. 4-8 (a) Half circular lamp reflector (b) Configurations of the circular lamp reflector and the free-form reflector

Two-dimensional and cross-sectional illuminance distribution charts are shown

in Fig. 4-9. The uniformity deviation was within 5% and the average illuminance was 167 (Lux), which was brighter and more uniform than the previous case without the lamp reflector.

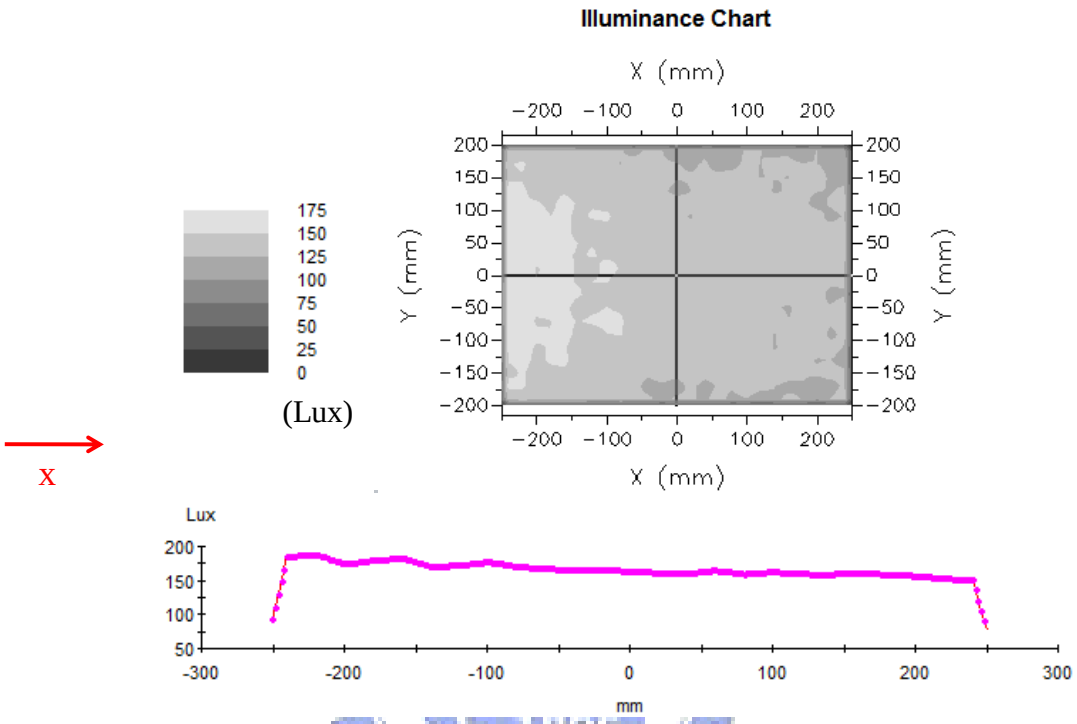

Fig. 4-9 Two-dimensional and cross-sectional illuminance distribution charts of the illumination system composed of circular lamp reflector and the free-form reflector

Table 4-1 Summary of average illuminance and uniformity deviation

	Average illuminance (Lux)	**Uniformity deviation (%)**
CCFL directly illuminating	63	34
Free-form reflector	111	8
Free-form reflector and lamp reflector	167	5

4.6 Faceted analysis

To implement the free-form surface reflector in manufacturing, the feasibility of combining faceted surface reflectors instead of continuous surface reflector was analyzed. The performance of faceted reflectors was modeled and analyzed through LightTools, which significantly reduced reliance on prototypes and design costs.

The shape of the free-form reflector shown in Fig. 4-4 was analyzed. This free-form continuous surface was divided into several planar faceted surfaces corresponding to the partition angle Δα as defined in Fig. 4-10. From the two-dimensional analysis viewpoint, each point is connected by a straight line.

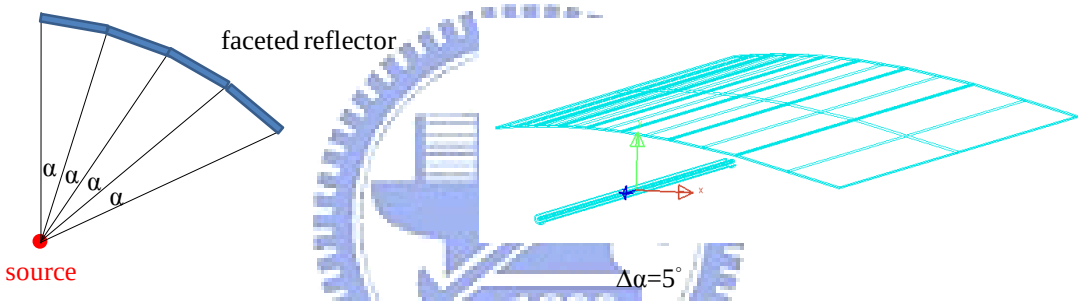

Fig. 4-10 Faceted surface reflectors

Illuminance distribution charts as well as illumination uniformity deviation of the faceted reflectors for different partition angles Δα, Δα is 10°, 5°, 2°, 1°, are shown in Fig. 4-11 and Table 4-2.

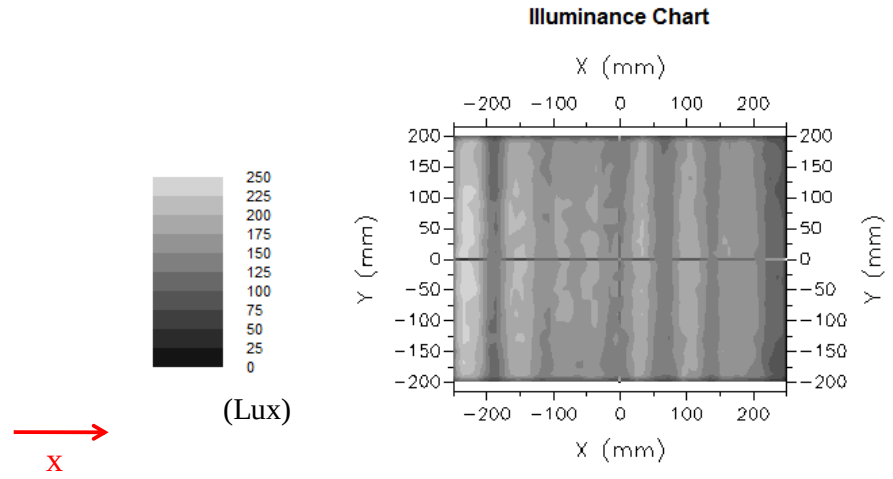
Illuminance Chart
X (mm)
Y (mm)
250
225
200
175
150
125
100
75
50
25
0
(Lux)
X

(a) α=10°

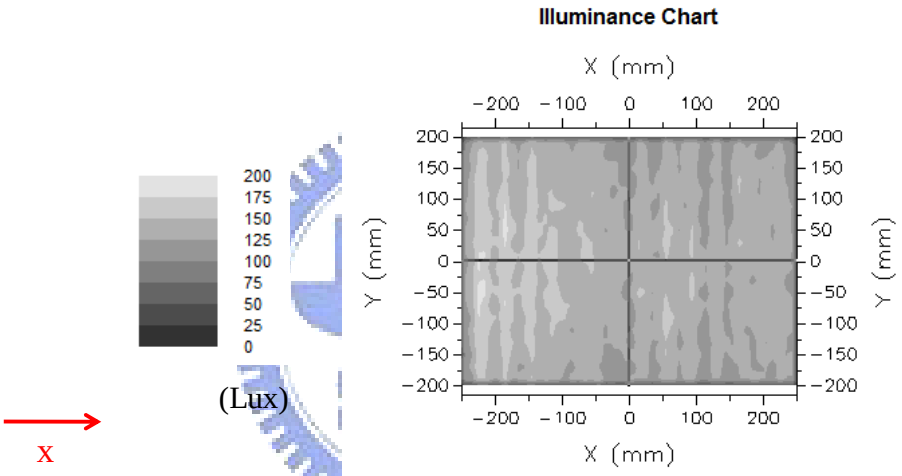
Illuminance Chart
X (mm)
Y (mm)
200
175
150
125
100
75
50
25
0
(Lux)
X

(b) α=5°

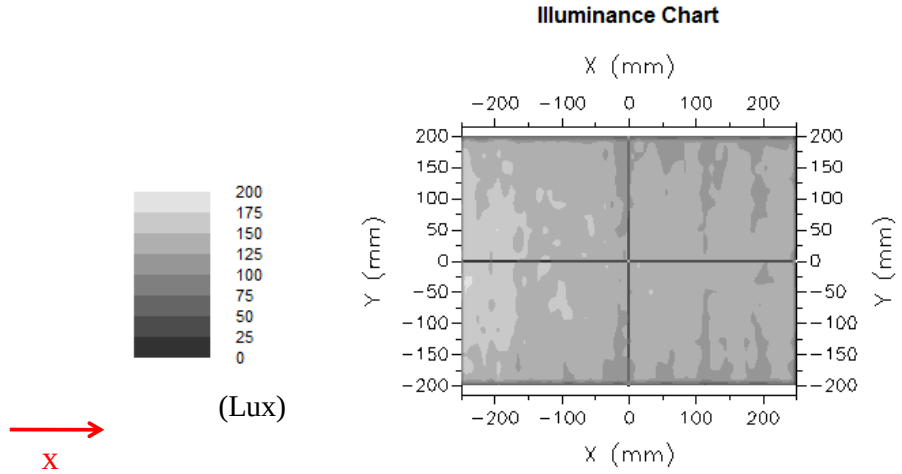
Illuminance Chart
X (mm)
Y (mm)
200
175
150
125
100
75
50
25
0
(Lux)
X

(c) α=2°

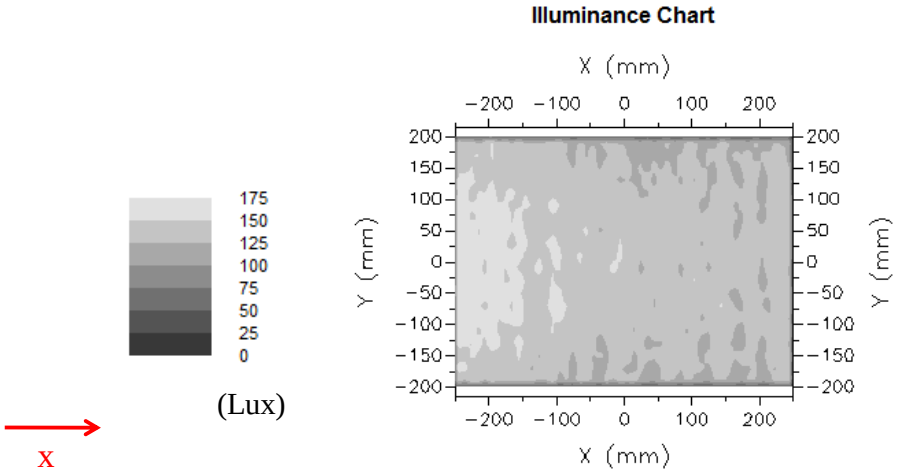

(d) α=1°

Fig. 4-11 Illuminance distribution charts of faceted reflectors for different partition angles Δα, Δα is 10°, 5°, 2°, 1°, respectively

Table 4-2 Average illuminance and uniformity deviation of faceted surface reflectors for different partition angles Δα

Δα (degree)	**Average illuminance (Lux)**	**Uniformity deviation (%)**
1	168	5
2	167	6
5	167	7
10	168	13

According to the simulation results, the uniformity deviation is more close to the continuous surface when the resolution of partition angle Δα is higher. The uniformity deviation is around 5% for the 1 degree partition, which is almost the same as the uniformity deviation of the continuous surface.

Cross-sectional illuminance distribution between faceted surface reflectors (the 1 degree partition) and the continuous surface reflector are compared in Fig. 4-12. According to Fig. 4-11 and Fig. 4-12, some dark and bright stripes appear across the illuminance distribution, due to the reasons that rays striking the edge of the faceted

reflector reflects to stray directions, and the faceted segments seriously deviate from continuous path when the angle θ is larger. Smaller partition angle Δα might relieve dark and bright stripes problems.

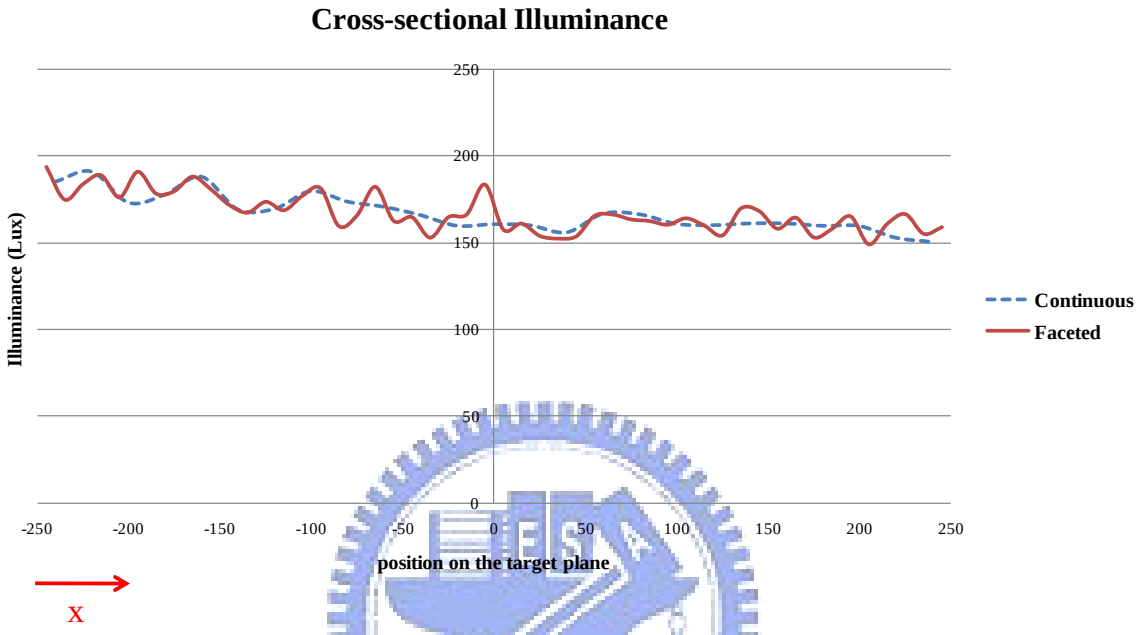

Fig. 4-12 Comparison of cross-sectional illuminance distribution between faceted surface reflectors (Δα=1°) and the continuous surface reflector

4.7 Discussion

In terms of simulation results in section 4.5, in order to improve illuminance on the target plane, some free-form reflector solutions for the same illuminated target plane were analyzed.

According to the mathematical model in Fig. 4-2, the reflector curve starts from the origin and extends in the positive x direction. The reflector only utilizes the source-emitted light which ranges from 0 degree to around 80 degrees. To increase the

use range of emitted light, another reflector extends in the negative x direction, which uses the light ranging from 0 degree to around -80 degree. Thus, the reflectors extend in the positive and negative x directions. Both negative and positive x direction reflectors redistribute light to the entire illuminated region, and the reflector curves are plotted in Fig. 4-13. The superposition of the illuminated light from the two reflectors is shown in Fig. 4-14. However, this illumination system suffers the serious issue of shadow of CCFL.

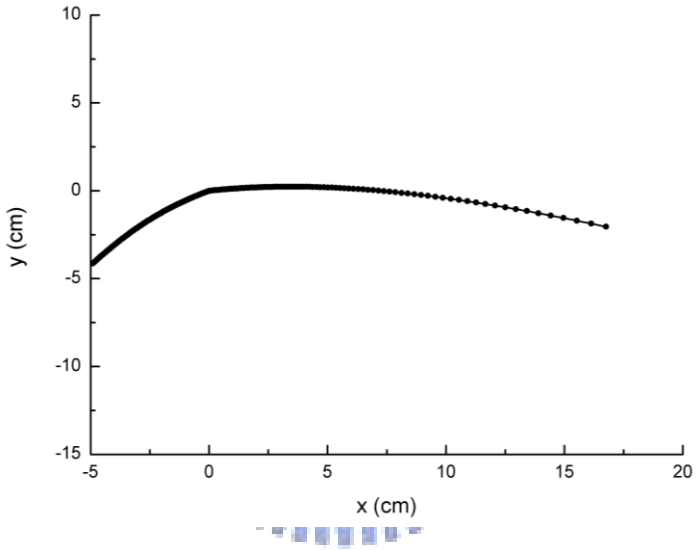

Fig. 4-13 Reflector curves extend in both the positive and negative x directions

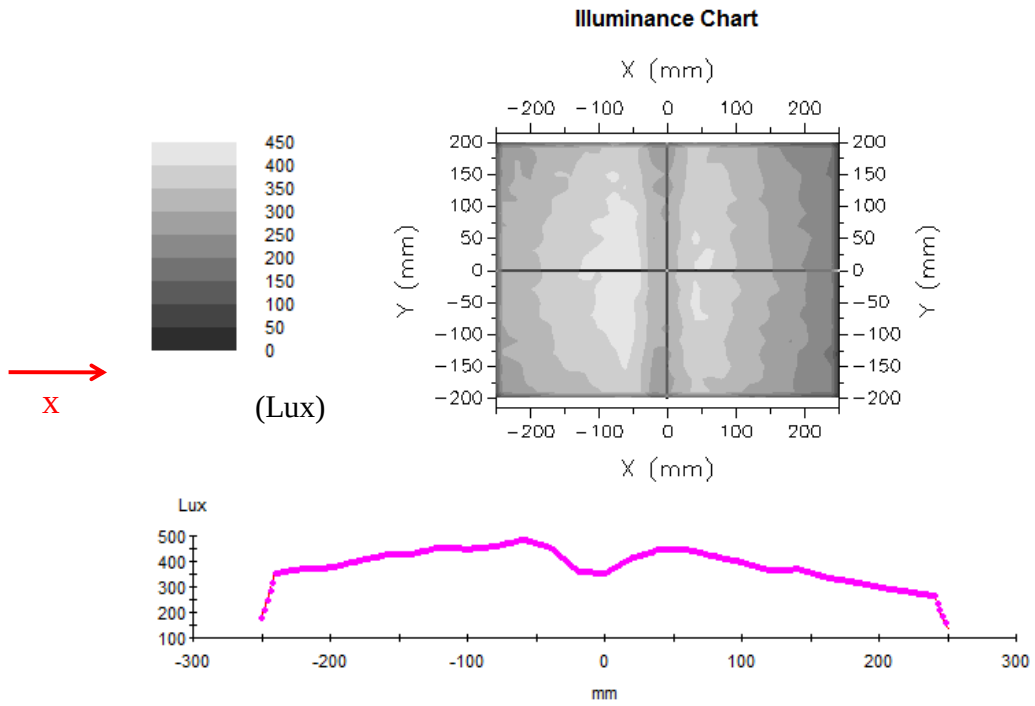

Fig. 4-14 Illuminance distribution charts of superposition of the illuminated light from the two reflectors which extend in both the positive and negative x directions

Furthermore, to solve the lamp shadow issue, by interchanging X(0°) and X(-80°), the negative x direction reflector reflects light and crosses light rays to redistribute on the illuminated region as shown in Fig. 4-15. The negative x direction reflector curve changes slightly (Fig. 4-16) and the simulation results are shown in Fig. 4-17. Compared to the previous design, the illuminance distribution becomes more uniform.

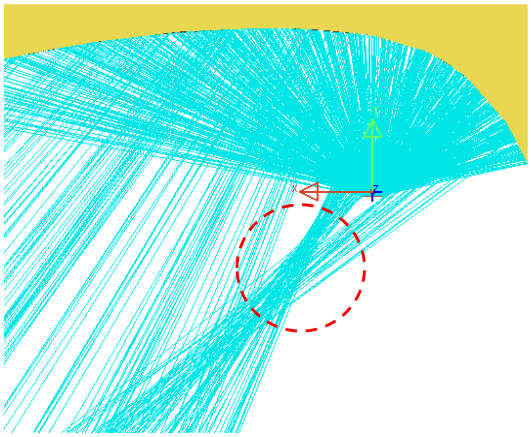

Fig. 4-15 Ray-tracing results of light rays cross

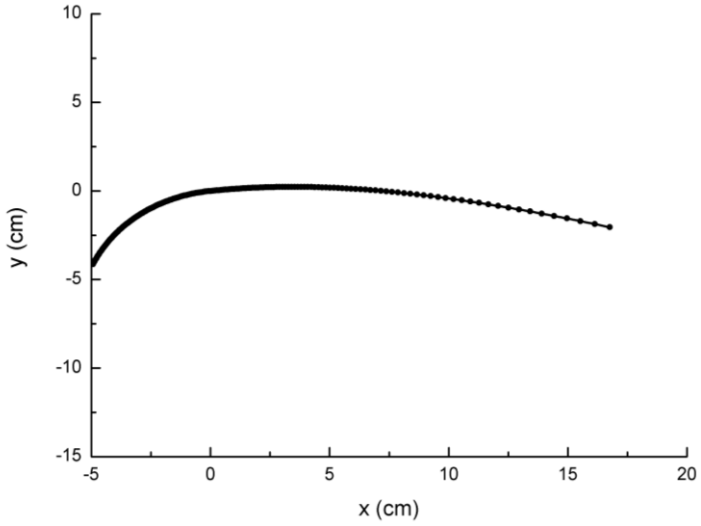

Fig. 4-16 Reflector curves for the superposition of the crossed light rays

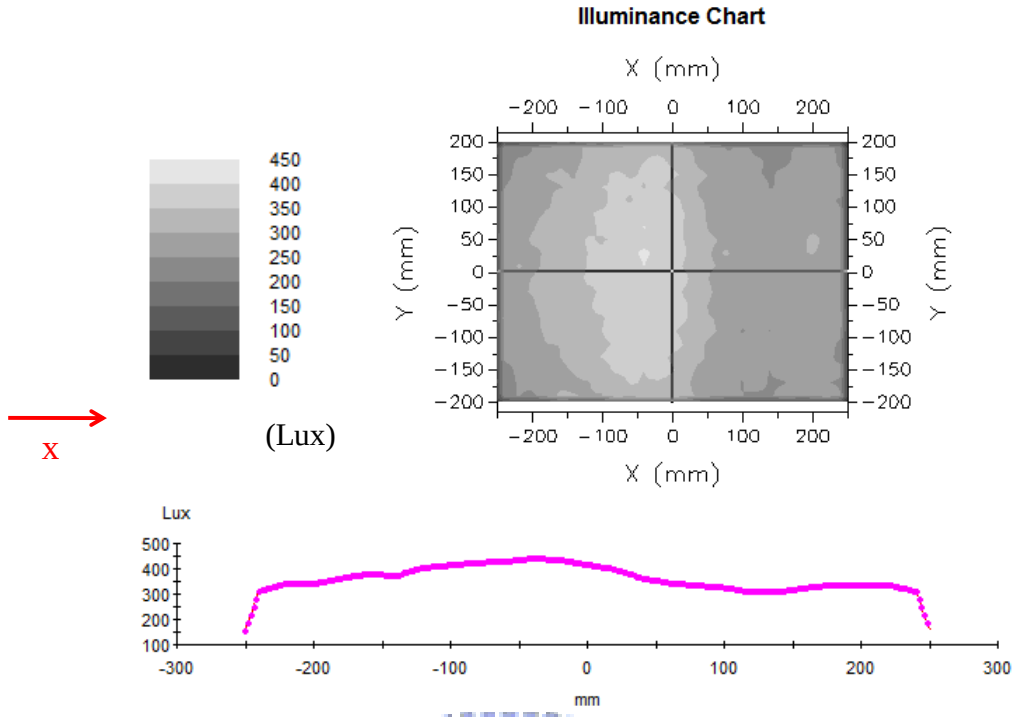

Fig. 4-17 Illuminance distribution charts of superposition of the crossed light rays

Chapter 5

Fabrication and Experiment

To implement the free-form reflector of Luminaire, a simple Luminaire prototype was fabricated for demonstration. Discussions on experimental results are stated as follows.

5.1 Fabrication technologies and results

5.1.1 Computer Numerical Controlled (CNC) machine [16][17]

Numerical Control is a method of automatically operating a manufacturing machine based on a code of letters, numbers, and special characters. A program is a complete set of coded instructions for executing an operation. The program is translated into corresponding electrical signals for input to motors which run the machine. A computer numerical control (CNC) machine is an NC machine with an on-board computer.

Today, most CNC machines are equipped with continuous-path controllers. Controllers cause the tool to maintain continuous contact with the part when the tool cuts a contour shape. Continuous-path operations include milling along lines at any angle, milling arcs, and lathe turning as shown in Fig. 5-1. Continuous-path controllers output motion by interpolating each position of the tool. The interpolated positions are determined such that they differ from the exact positions within an acceptable tolerance. Many continuous-path controllers interpolate curves as a series of straight-line segments. Smaller line segments can achieve high accuracy. (Fig. 5-2)

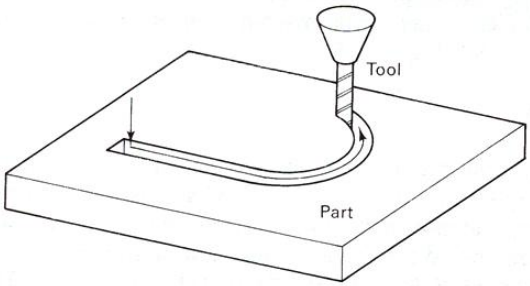

Fig. 5-1 Continuous-path tool movement

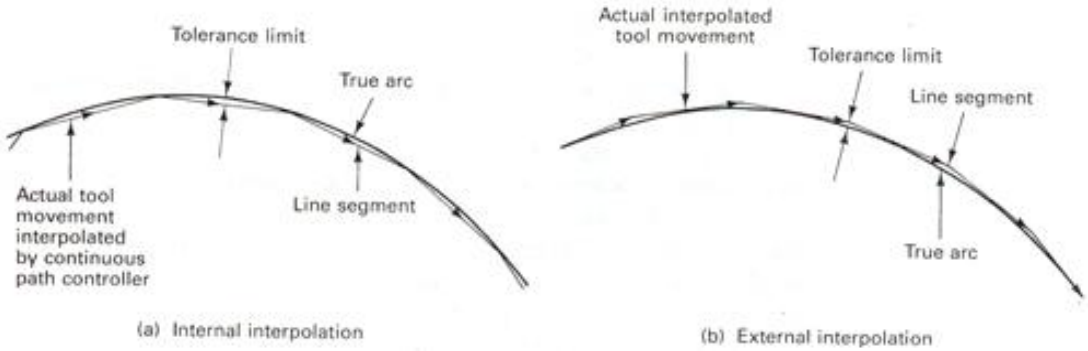

Fig. 5-2 Interpolation for continuous-path movement

The CNC lathe is a machine tool that is designed to remove material from stock which is clamped and rotated around an axis. Most metal cutting is done with a sharp single-point cutting tool. Modern CNC lathes use turrets to rigidly hold and move cutting tools. A typical CNC turret lathe or turning center is shown in Fig. 5-3.

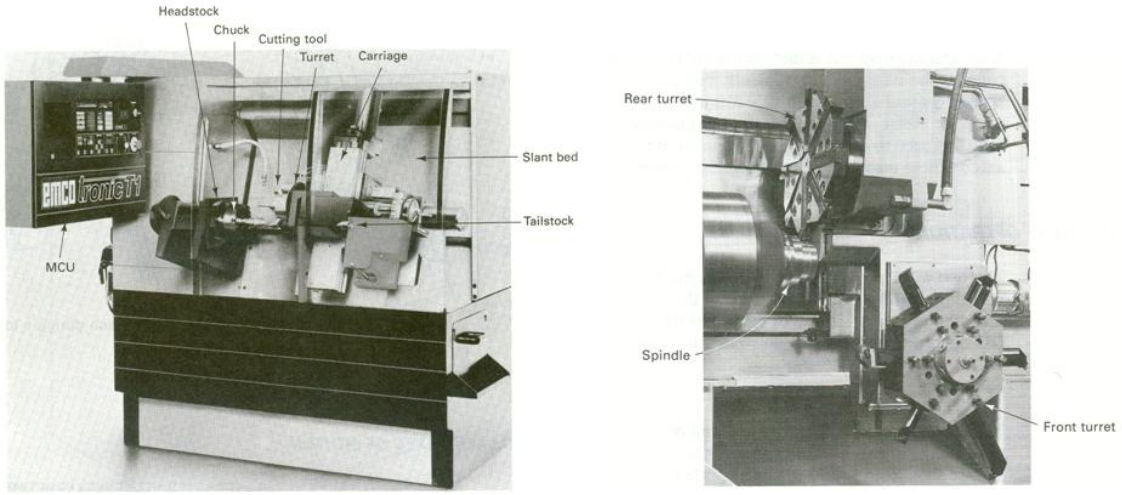

Fig. 5-3 CNC lathe

In modern CNC systems, end-to-end component design is highly automated using CAD/CAM programs. The programs produce a computer file that is interpreted to extract the commands needed to operate a particular machine, and then loaded into the CNC machines for production.

5.1.2 Luminaire prototype results

The free-form reflector shape for the Luminaire prototype is depicted in Fig. 4-4. The free-form surface was modeled by CNC manufacturing methods. Then a specular sheet with high reflectivity was adhered to the model surface through an optical adhesive. Two CCFLs were utilized to enhance illuminance. Fig. 5-4 shows pictures taken of the prototype.

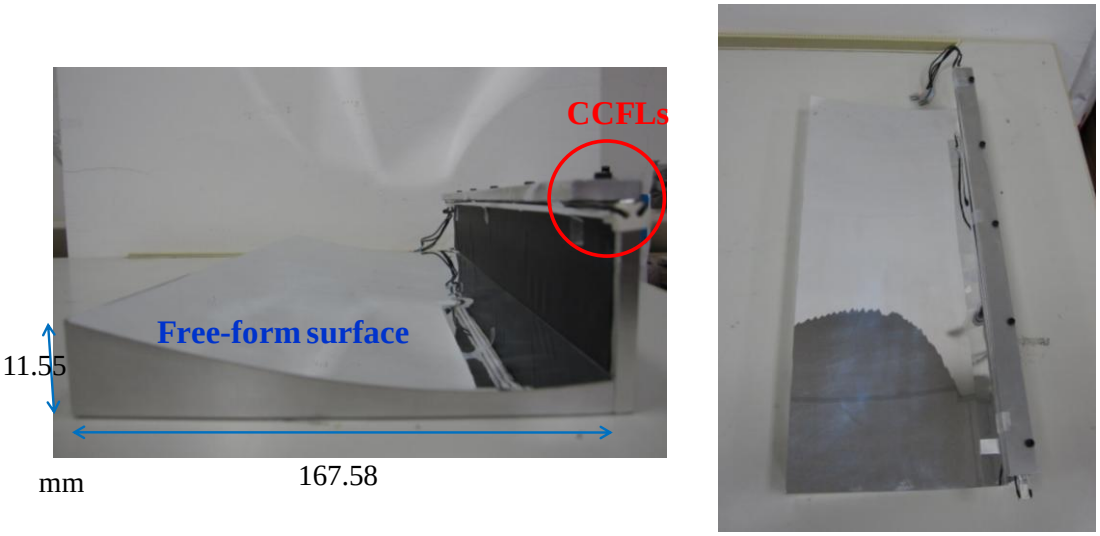

Fig. 5-4 Luminaire prototype

5.2 Instrument and Measurement setup

5.2.1 Instrument

PM Series™ Imaging Colorimeter and Photometer [18] (Fig. 5-5) was utilized as the instrument to measure light distribution on the target plane. ProMetric systems are capable of capturing images and quantitatively analyzing each individual pixel in these images for its photometric, radiometric and colorimetric characteristics. ProMetric instruments consist of a CCD (Charge-Coupled Device) based camera system, together with instrument control, data acquisition and image processing software.

Fig. 5-5 PM Series™ Imaging Colorimeter and Photometer

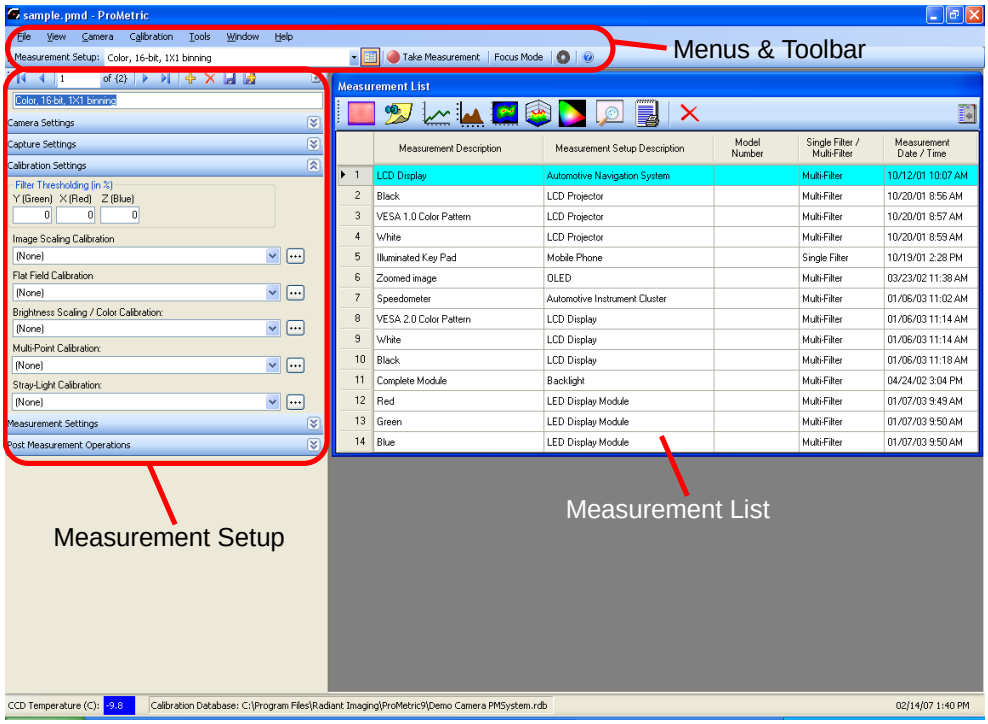

Fig. 5-6 ProMetric software interface

5.2.2 Measurement setup

The measurement setup is illustrated in Fig. 5-7. For convenience, the Luminaire prototype was put in front and below a target plane when light illuminated the target plane. The target plane was a diffuse surface (white paper). CCD camera was positioned in front of the target plane, and the luminance distribution on the target plane was captured by the CCD camera.

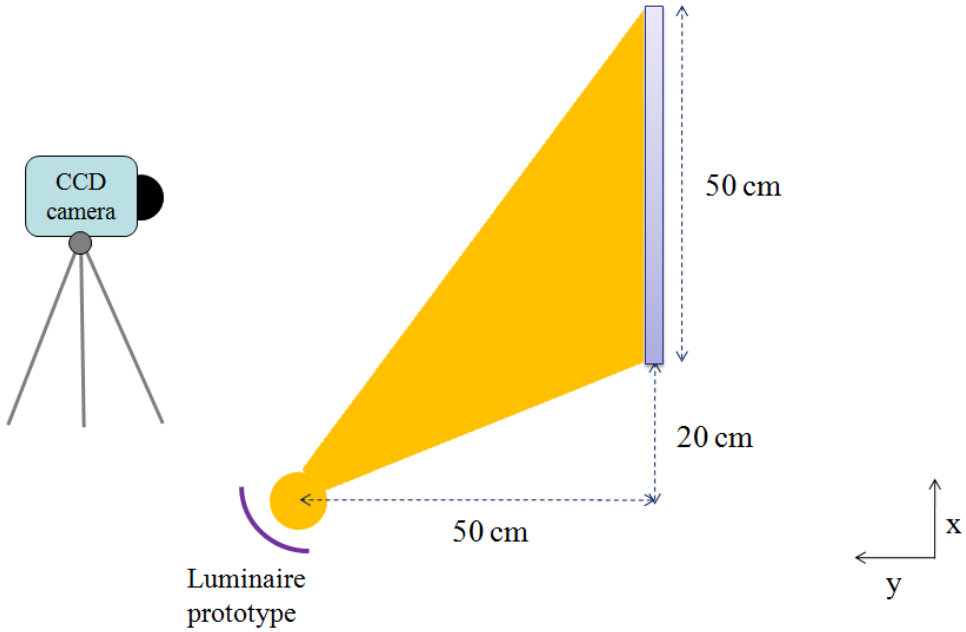

Fig. 5-7 CCD camera measurement setup

5.3 Experimental results and discussions

5.3.1 Experimental results

According to the measurement setup illustrated in Fig. 5-7, luminance distribution on the target plane from the Luminaire prototype is shown in Fig. 5-8. The color bar represents the luminance distribution which was normalized by the maximum value. ($\frac{\text{Luminance}}{\text{maximum Luminance}} \times 100\%$) By comparison, the normalized luminance distribution result of the conventional Luminaire, whose luminaire reflector is not specified for uniform lighting purpose, is shown in Fig. 5-9. Cross-sectional normalized luminance distribution of the Luminaire prototype and the conventional Luminaire are shown in Fig. 5-10 and Fig. 5-11, respectively.

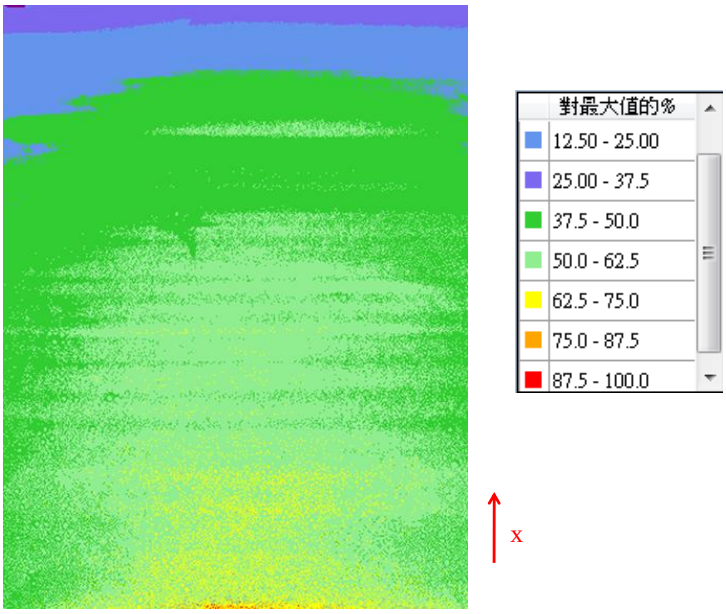

Fig. 5-8 Luminance distribution of proposed Luminaire prototype

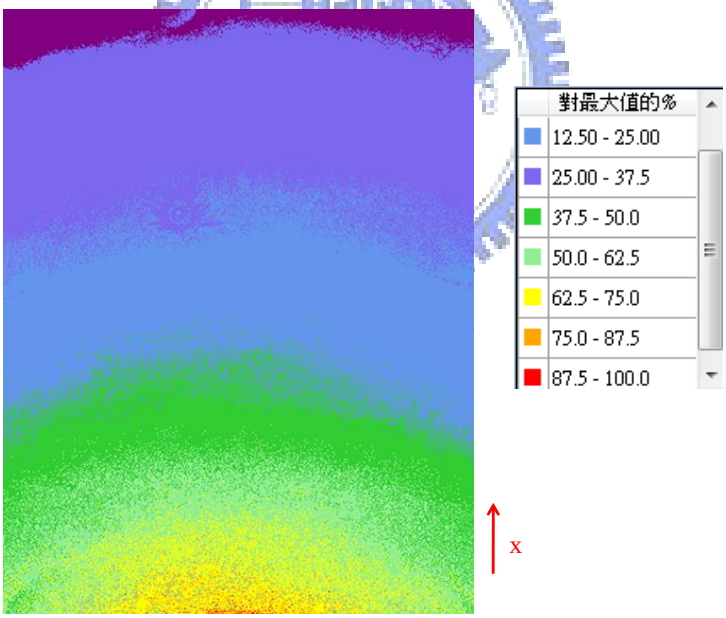

Fig. 5-9 Luminance distribution of the conventional Luminaire

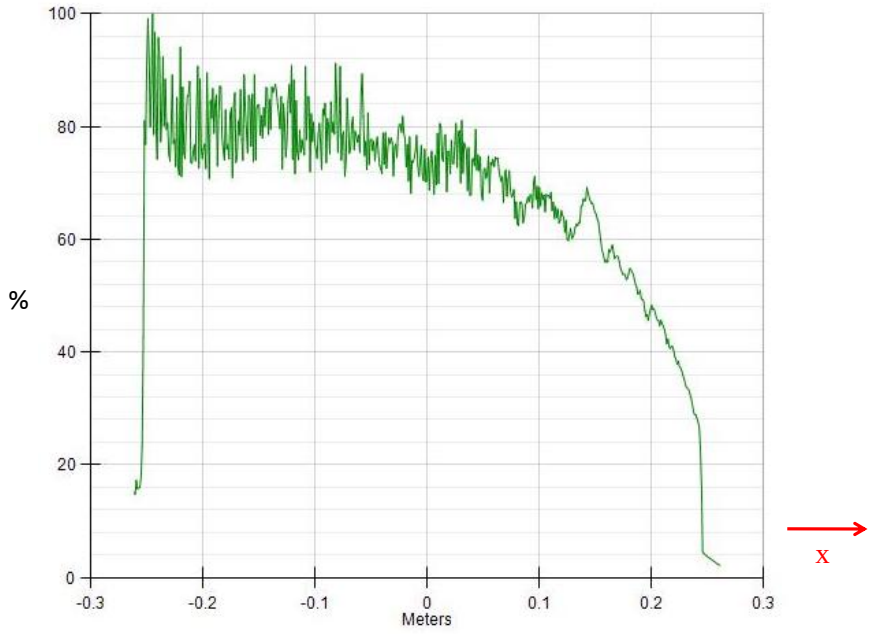

Fig. 5-10 Cross-sectional normalized luminance distribution of the Luminaire prototype

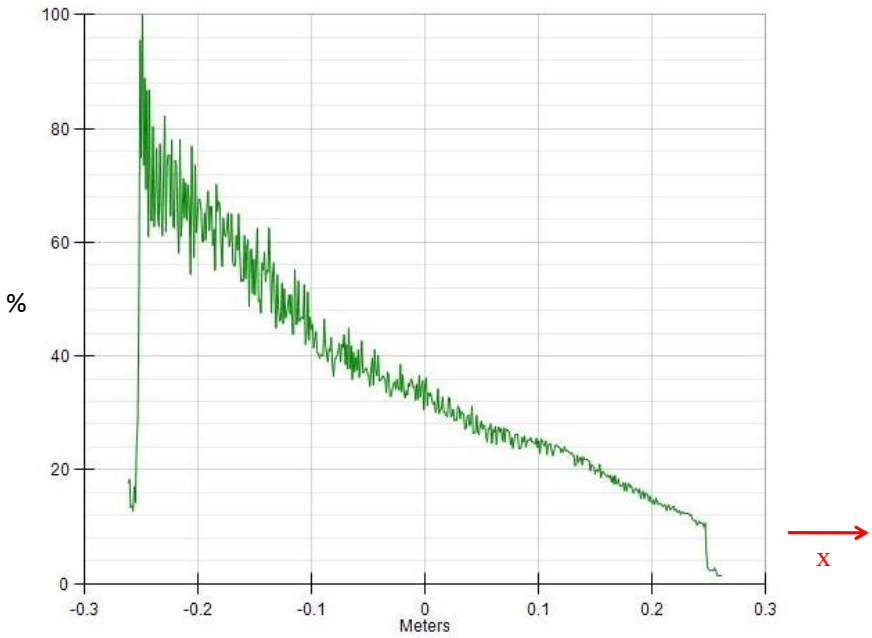

Fig. 5-11 Cross-sectional normalized luminance distribution of the conventional Luminaire

Furthermore, Light Meter was used to measure illuminance (Lux) on the target plane. Several points on the plane were chosen as measuring positions. Comparison of cross-sectional illuminance results between the conventional Luminaire and the Luminaire prototype are shown in Fig. 5-12.

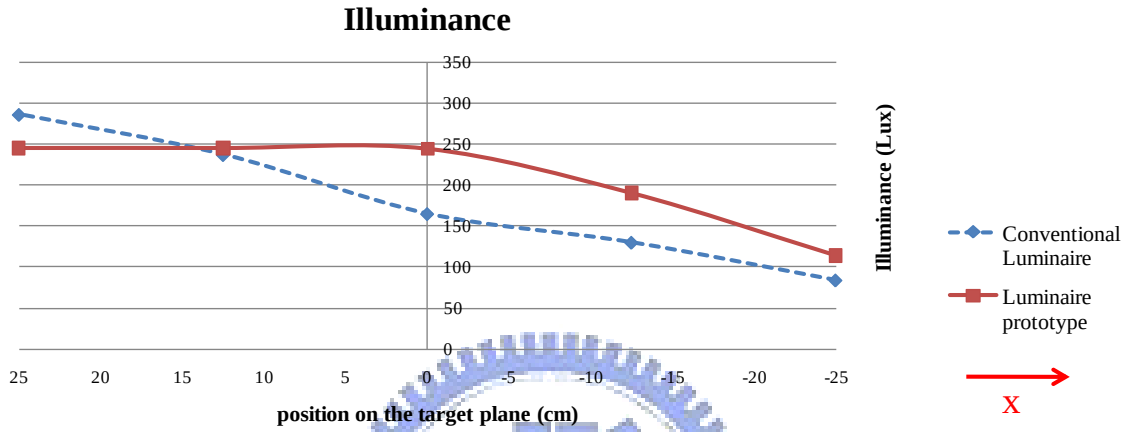

Fig. 5-12 Comparison of cross-sectional illuminance results between the conventional Luminaire and the Luminaire prototype

5.3.2 Discussion

According to the above results, uniformity deviation of the Luminaire prototype is 14.5% while uniformity deviation of the conventional Luminaire is about 40%. The proposed Luminaire obviously improved illumination uniformity, except that there were certain issues due to fabrication errors.

The illuminance on the target plane was lower along the positive x direction. Since CNC Lathe dimension tolerance was ±0.03 mm, interpolating and cutting errors for the reflector surface were more sensitive to a large angle θ incidence, resulting in darker region. Besides, there were errors during the process of adhering the specular sheet to the model surface, for example, mismatch and bubble, which changed optical

property for the reflecting surface. Moreover, two CCFLs were utilized in the Luminaire prototype to improve average illuminance, so the output light distribution from sources slightly deviated from the calculated model.

Some dark and bright stripes appeared across the luminance distribution. This phenomenon resulted from scratches and notches on the model surface as shown in Fig. 5-13. These scratches and notches were created due to cutting errors. Rays struck these scratches and notches and then reflected to different directions. The result was similar to the faceted surface reflector analysis in section 4.6.

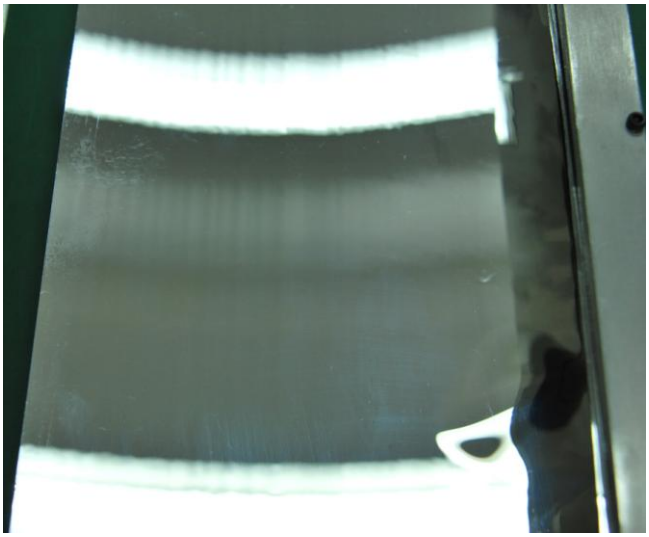

Fig. 5-13 Scratches and notches on the model surface

5.4 Performance of lighting upon a reflective display

The merits of the Luminaire prototype lighting upon a reflective display was evaluated. Light emitted from the Luminaire prototype illuminated a Cholesteric LCD and a poster, respectively. Results of the Luminaire prototype were compared with that

of the conventional Luminaire which is not specified for uniform lighting purpose.

The lighting performance results on the Cholesteric LCD are shown in Fig. 5-14, and results on the poster are shown in Fig. 5-15.

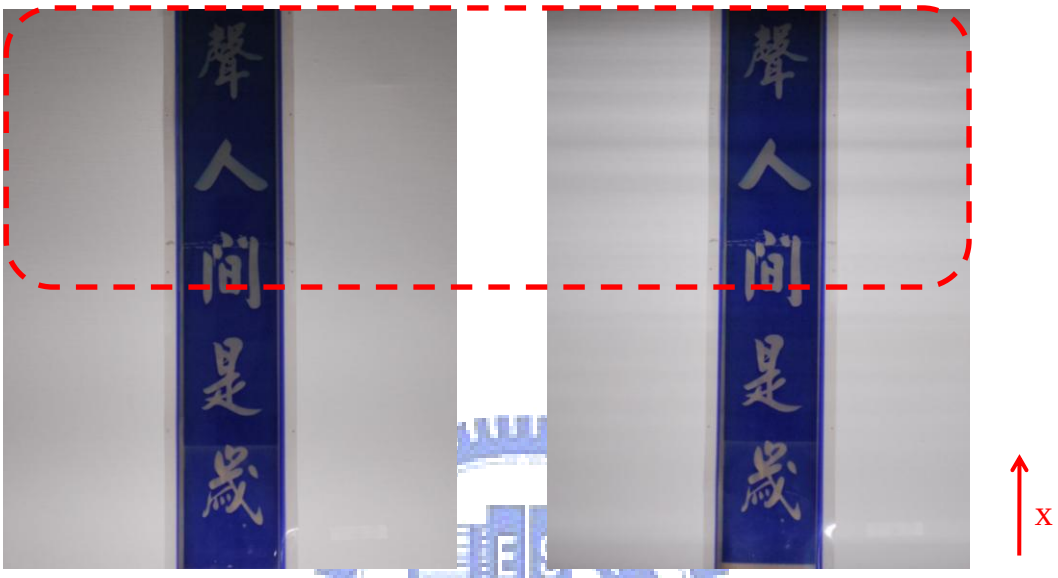

(a) Conventional Luminaire (b) Proposed Luminaire prototype

Fig. 5-14 Comparison of lighting performance on the Cholesteric LCD (a) the conventional Luminaire (b) the proposed Luminaire prototype

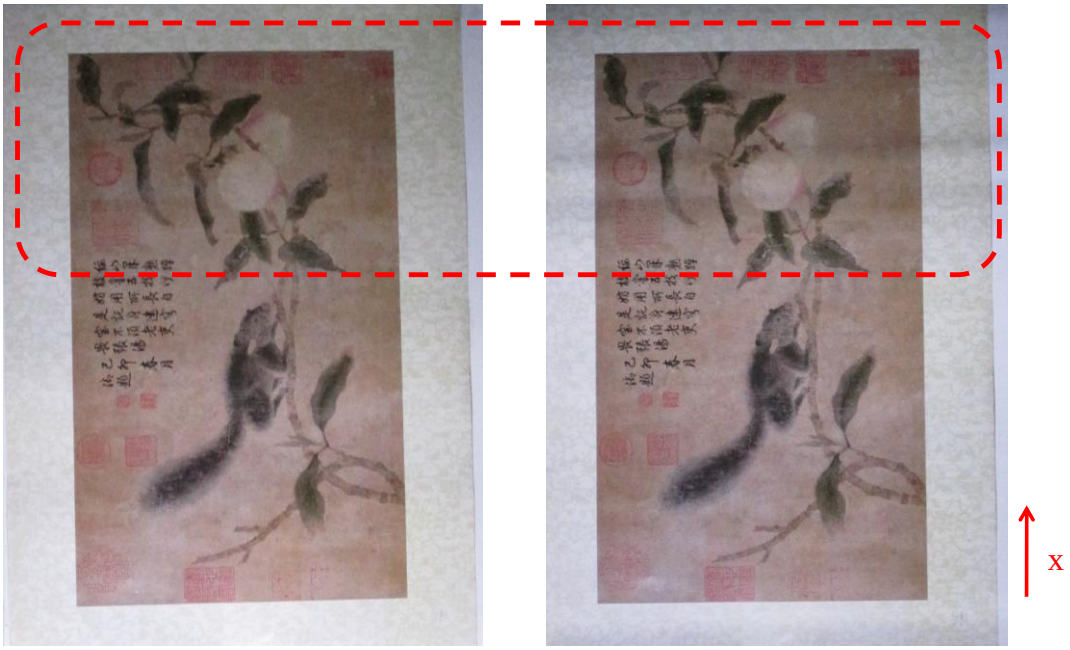

(a) Conventional Luminaire (b) Proposed Luminaire prototype

Fig. 5-15 Comparison of lighting performance on the poster (a) the conventional Luminaire (b) proposed Luminaire prototype

From the above pictures, comparing the Luminaire prototype with the conventional Luminaire, uniformity improvement perceived by the human eye was not as significant as the results captured by the CCD camera. This is because of adaption to brightness by the human eye, so the difference between maximum and minimum luminance was not seen. The issue can be further improved by utilizing CCFL that emits higher flux. The difference will become distinguishable when the illuminance level is raised.

In addition, there were still perceivable dark and bright stripes on the display from the Luminaire prototype, which resulted from fabrication errors discussed in section 5.3.

Chapter 6

Conclusions and Prospects

Reflective LCDs, without back-light, utilize ambient light to display images. With progress in display technologies, reflective LCDs have been applied to electric billboards and electric posters. The image qualities are ideal in well-lit locations or under diffuse sunlight. At night or in dim indoor environments, front lighting is required due to insufficient surrounding illumination. Conventional front lighting Luminaires for the large-size reflective displays generally suffer issues of non-uniform illumination, resulting in poor image quality.

In this thesis, the front illuminating system for uniform illumination on the target display was proposed and studied. A free-form mirror reflector redistributed light from CCFL source. The shape of the free-form reflector was numerically calculated according to the normal distance between the source and the target plane, the illuminated region, and the positions of the source and the target plane. For the practical design case, the parameters were shown in Fig. 4-1 when z= 50 cm.

Based on simulation results, compared to CCFL directly illuminating case, the proposed illumination system consisted of the free-form reflector improved illumination uniformity while uniformity deviation was within 5%. The average illuminance was 167 Lux.

According to faceted analysis for free-form reflector surface, the uniformity deviation was more close to the continuous surface reflector when the partition angle $\Delta\alpha$ was smaller. Furthermore, smaller partition angle $\Delta\alpha$ might relieve dark and bright

stripes problems.

A simple Luminaire prototype was fabricated for demonstration. The free-form surface was modeled by CNC manufacturing methods. Then a specular sheet with high reflectivity was adhered to the model surface through an optical adhesive. Two CCFLs were used to enhance illuminance.

Experimental results for the luminance distribution on the target plane captured by CCD camera verified uniformity improvement (uniformity deviation δ=14.5%), except the issues due to fabrication errors including interpolating and cutting errors, which were limited to accuracy of utilized manufacturing methods.

6.1 Limitations of the front illuminating system

There are some limitations to reflector design based on the linear model. Referred to Fig. 3-3 and equation (3.8), illuminating point on the target plane $X(\theta)$ is linear to incident ray angle θ, which was accurate in mathematical description. However, in view of Radiometry, the illuminating ray projection angles on the plane are slightly different as shown in Fig. 4-5, leading to brightness variation between upper and lower plane. Thus, the brightness on the lower plane will decrease when the illuminating ray projection angles are seriously deviated from those on the upper plane. In addition, the reflector in the proposed illumination system only utilizes the source-emitted light which ranges from 0 degree to around 80 degrees. Simulation results in section 4.7 showed that the reflectors extend in both the positive and the negative x directions increased the use range of emitted light, but they suffered the issue of CCFL shadow. The issue remains as the future work.

6.2 Future work

For fabricating the Luminaire prototype, interpolating and cutting errors for the reflector shape can be improved by using CNC machines with smaller dimension tolerance. Reflector shape with higher accuracy can control ray-directions precisely. Scratches and notches on the reflector surface can be alleviated through surface treatment or optical adhesive. High flux output CCFL is preferable to enhance illumination level.

In fact, the process of adhering the specular sheet to the model surface will cause reflecting properties to change slightly. Instead of adhering the specular sheet, coating a layer of high-reflective material on the model surface is an alternative.

Furthermore, considering the specular reflection issue for the Cholesteric LCD surface, microstructure design can be applied to redirect light to the viewing requirement. The additional prism array film can be attached to the front surface of the Ch-LCD to redirect the light distribution and enhance the image quality.

Reference

[1] http://en.wikipedia.org/wiki/File:Scooter_headlights.jpg

[2] http://www.parc.com/research/publications/files/5706.pdf

[3] Andreas Timinger et al. Designing Tailored Free-Form Surfaces for General Illumination, Proc. of SPIE Vol. 5186 (2003)

[4] New Buildings Institute, Inc. Advanced Lighting Guidelines (2003)

[5] Yi-Pai Huang, Applications of Microoptical Components for Image Quality Enhancing on Portable Liquid Crystal Displays, PhD thesis, NCTU(2004)

[6] Magink display technologies, http://www.magink.com/

[7] Bahaa E. A. Saleh and Malvin Carl Teich, Fundamentals of Photonics, John Wiley & Sons, Inc, p.4 (1991)

[8] Frank J. Pedrotti and Leno S. Pedrotti, Introduction to Optics, Prentice Hall, p.10-15 (1992)

[9] http://note.j-i-n.name/2005/06/photopic-luminous-efficiency-function

[10] Roland Winston, Juan C. Minano and Pablo Benitez, Nonimaging Optics, Elsevier Academic Press, p.415-418 (2005)

[11] Yankun Zhen, Zhenan Jia, Wenzi Zhang, The Optimal Design of TIR Lens for Improving LED Illumination Uniformity and Efficiency, Proc. of SPIE Vol. 6834, 68342K, (2007)

[12] Kuan-Ting Chen, The Design of Illumination System and its Applications to UV Illumination, Mater thesis, NCTU (2007)

[13] http://en.wikipedia.org/wiki/Runge-Kutta

[14] Kendall Atkinson, Elementary Numerical Analysis 2nd edition, p. 329-330 (1993)

[15] Optical Research Associates, http://www.opticalres.com/index.html

[16] James V. Valentino and Joseph Goldenberg, Introduction to computer numerical control, Prentice Hall

[17] http://en.wikipedia.org/wiki/CNC

[18] ProMetric™ 9.1, http://www.radiantimaging.com/